

PHASE DIAGRAM OF A MODIFIED XY MODEL

BACHELOR THESIS

Jakub Imriška

COMENIUS UNIVERSITY IN BRATISLAVA
FACULTY OF MATHEMATICS, PHYSICS AND INFORMATICS
DEPARTMENT OF EXPERIMENTAL PHYSICS



Study Programme: Physics 4.1.1

Advisor: Doc. RNDr. Richard Hlubina, DrSc

Bratislava, 2009

I would like to thank to my advisor Doc. RNDr. Richard Hlubina, DrSc for his almost inexhaustible patience, professional guidance and miscellaneous support, which I personally highly appreciate.

Abstract

Author: Jakub Imriška
Title: Phase diagram of a modified XY model
Type of thesis: Bachelor thesis
University: Comenius University in Bratislava
Faculty: Faculty of Mathematics, Physics and Informatics
Department: Department of Experimental Physics
Study Programme: Physics 4.1.1
Advisor: Doc. RNDr. Richard Hlubina, DrSc

We study a modified 2-dimensional XY model on the square lattice defined by the Hamiltonian

$$H = - \sum_{\langle kl \rangle} [J_1 \cos(\theta_k - \theta_l) + J_2 \cos 2(\theta_k - \theta_l)], \quad \text{for } J_2 \geq 0,$$

using Monte Carlo simulations. Our goal is to specify the phases in the space of parameter $j = \frac{J_1}{J_1 + 4J_2}$ and temperature T and to determine the types of phase transitions between the phases. Our results indicate that the phase diagram consists of 3 phases (magnetic, nematic and paramagnetic). The transition between the magnetic and the paramagnetic phase is of the Kosterlitz-Thouless (KT) type with an universal jump $\frac{2T}{\pi}$ caused by unbinding of vortex pairs. The nematic-paramagnetic transition is of the KT type with an universal jump $\frac{8T}{\pi}$ caused by unbinding of half-vortex pairs. The transition between the magnetic and the nematic phase is of the Ising type.

keywords: modified XY model, Kosterlitz-Thouless phase transition, phase diagram, Monte Carlo simulation, Ising phase transition, phase diagram.

Contents

Abstract	3
1 Introduction	5
1.1 The 2-dimensional XY model	5
1.2 Modified XY model	5
1.2.1 Similarity between $j = 0$ and $j = 1$	6
1.2.2 Similarity between J_1 and $-J_1$	7
1.2.3 Expectations	7
2 KT phase transition	9
2.1 The KT magnetic-paramagnetic phase transition	9
2.1.1 Vorticity	10
2.1.2 Spin-wave solution	10
2.1.3 Vortex	10
2.1.4 Independence of spin waves and vortices	13
2.1.5 2D electrostatics	13
2.2 KT equations	14
2.3 The KT nematic-paramagnetic phase transition	16
2.4 Renormalization of J due to anharmonicity	17
2.5 Renormalization of J due to vortex unbinding	19
3 Monte Carlo simulation	20
3.1 The Metropolis algorithm	21
3.2 The Wolff algorithm	21
3.3 Autocorrelation time and error of the mean	23
3.4 Measured observables	23
3.5 Specific heat	25
3.6 Helicity modulus	25
3.7 Susceptibilities	27
3.8 Identification of the KT phase transition	27
4 Results of numerical experiments	29
4.1 Numerical results for $j = 1$	29
4.2 Numerical results for $j = 0$	31
4.3 Numerical results for $j = 0.02$	31
4.4 Numerical results for $j = 0.16$	36
4.5 The phase diagram	36
Conclusion	40
Slovak summary - Slovenský súhrn	41

Chapter 1

Introduction

1.1 The 2-dimensional XY model

The 2-dimensional (2-D) XY model on the square lattice is defined by the Hamiltonian

$$H_{XY} = -J_1 \sum_{\langle kl \rangle} \cos(\theta_k - \theta_l), \quad (1.1)$$

where the indices k and l numerate the lattice sites on a 2-dimensional square lattice, the sum is over the nearest-neighbour lattice sites and θ_k is the angle associated with each site. This model might be realized by spins localized on a 2-D square lattice fixed in the lattice plane.

The long-wavelength lattice waves are responsible for destroying the long-range order in the 2-D models [1].¹ Nevertheless, there might exist a low-temperature phase with “quasi”-long-range order.² Kosterlitz and Thouless have shown that the model undergoes a Kosterlitz-Thouless (KT) phase transition from the “quasi”-ordered into a disordered high-temperature phase [2]. The phase transition occurs at a temperature, when tightly bound topological defects (pairs of vortex and anti-vortex) unbind and become free.

1.2 Modified XY model

Our modified model is defined by the Hamiltonian

$$H = - \sum_{\langle kl \rangle} [J_1 \cos(\theta_k - \theta_l) + J_2 \cos 2(\theta_k - \theta_l)], \quad (1.2)$$

where J_2 is considered to be non-negative. The modified model appeared to be important in the context of “possible vortex splitting in high-temperature cuprate superconductors” [3]. The Hamiltonian Eq.(1.2) may be, equivalently, rewritten into

$$H = -J \sum_{\langle kl \rangle} \left[j \cos(\theta_k - \theta_l) + \frac{1-j}{4} \cos 2(\theta_k - \theta_l) \right], \quad (1.3)$$

where $J = J_1 + 4J_2$ is considered to be positive and the coupling parameter $j = \frac{J_1}{J}$ lies in the range $[0, 1]$.³ The choice for the unit J is motivated by the harmonic approximation of the Hamiltonian Eq.(1.3),

$$H - H_{\text{ground}} \approx \frac{J}{2} \sum_{\langle kl \rangle} (\theta_k - \theta_l)^2, \quad (1.4)$$

¹Which is an important difference between 2-D and 3-D models.

²The “quasi”-ordered phase will be referred to as a magnetic, and a nematic phase, although it would be more exact to call them “quasi”-magnetic, and “quasi”-nematic.

³The interaction with negative J_1 reproduces the same phases as positive J_1 . We show this later in Sec.1.2.2. Hence, our study concentrates on $j \in [0, 1]$, because j from that range reproduces any non-negative ratio $\frac{J_1}{J_2}$.

where $H_{\text{ground}} = -2JN^2(j + \frac{1-j}{4})$ is the energy of the ground state of the lattice. Note, that the low-temperature approximation has no dependency on j .

We will measure the temperature in most cases in units J .⁴ Sometimes it will be natural to use units J_2 instead of J , especially for comparing results from models with different j – the unit J is namely a function of j .

The function defining the energy of a single bond between the spins k and l is symmetric function (regarding indices k and l),

$$e(\theta_k, \theta_l) \equiv e(\theta_k - \theta_l) = -J[j \cos(\theta_k - \theta_l) + \frac{1-j}{4} \cos 2(\theta_k - \theta_l)]. \quad (1.5)$$

For theoretical purposes it is useful to analyse also the continuous model. For spacing $a \rightarrow 0^+$ is the harmonic approximation Eq.(1.4) exact. The Hamiltonian of the continuous “lattice” is

$$H - H_{\text{ground}} \approx \frac{J}{2} \sum_{\langle kl \rangle} (\theta_k - \theta_l)^2 \approx \frac{J}{2} \sum_k \left[\left(\frac{\partial \theta(\mathbf{r}_k)}{\partial x} a \right)^2 + \left(\frac{\partial \theta(\mathbf{r}_k)}{\partial y} a \right)^2 \right] \xrightarrow{a \rightarrow 0^+} \frac{J}{2} \int d^2r [\nabla \theta(\mathbf{r})]^2, \quad (1.6)$$

where $\theta(\mathbf{r})$ is the angle associated with the point \mathbf{r} . As one might have expected, the continuous model has again no dependency on j .

1.2.1 Similarity between $j = 0$ and $j = 1$.

In this section we denote the parameter j by an upper index. The Hamiltonians of the models with $j = 1$ and $j = 0$ are

$$H^{[1]}(\theta) = -J \sum_{\langle kl \rangle} \cos(\theta_k - \theta_l), \quad (1.7)$$

$$H^{[0]}(\theta) = -\frac{J}{4} \sum_{\langle kl \rangle} \cos 2(\theta_k - \theta_l). \quad (1.8)$$

The space of all possible configurations θ of a lattice $N \times N$ is $C \equiv [0, 2\pi)^n$, where $n \equiv N^2$. Equivalently, we may describe the space of all possible configurations θ in a different way, as an element of the space $C' \equiv C_1 \times C_2$, where $C_1 \equiv \{0, 1\}^n$ and $C_2 \equiv [0, \pi)^n$. Then the configuration $c' \equiv (\mathbf{p}, \mathbf{r}) \equiv (p_1, p_2, \dots, p_n, r_1, r_2, \dots, r_n) \in C'$; $p_i \in \{0, 1\}, r_i \in [0, \pi)$ is *encoding* the information $\theta_i = \pi p_i + r_i$.⁵ The advantage of this notation is that the energy $H^{[0]}$ does not depend on \mathbf{p} and may be expressed as

$$H^{[0]}(\mathbf{p}, \mathbf{r}) = H^{[0]}(\mathbf{r}) = \frac{1}{4} H^{[1]}(2\mathbf{r}), \quad (1.9)$$

where $2\mathbf{r}$ is an element of C .

The statistical sum for $j = 1$ is

$$Z^{[1]}(T) = \int_C \mathcal{D}\theta e^{-\frac{H^{[1]}(\theta)}{T}}. \quad (1.10)$$

where $\mathcal{D}\theta \equiv d^n\theta = \prod_i d\theta_i$ is an n -dimensional differential. The statistical sum for $j = 0$ is

$$Z^{[0]}(T) = \int_{C_2} \mathcal{D}\mathbf{r} 2^n e^{-\frac{H^{[0]}(\mathbf{r})}{T}} = \left[\begin{array}{c} \text{subst.} \\ \theta_i = 2\mathbf{r}_i \end{array} \right] = \int_C \mathcal{D}\theta e^{-\frac{H^{[1]}(\theta)}{4T}} = Z^{[1]}(4T). \quad (1.11)$$

That gives us a powerful tool. We define transformation $T_{\mathbf{p}} : C \rightarrow C$ as follows

$$T_{\mathbf{p}} : \theta_i \mapsto \pi p_i + \theta_i/2, \quad (1.12)$$

where $p_i \in \{0, 1\}$. Then for the probabilities hold

$$p^{[1]}[\theta, 4T] = \frac{1}{Z^{[1]}(4T)} e^{-\frac{H^{[1]}(\theta)}{4T}} = p^{[0]}[T_{\mathbf{p}}(\theta), T], \quad (1.13)$$

⁴As one my colleague suggested, it might be Joule as the unit of energy.

⁵Surely, both ways enable to describe any configuration and there is bijection between the 2 configuration spaces.

which guarantees that the phase in model with $j = 1$ at a certain temperature $4T$ will be the same, in the sense of transformation $T_{\mathbf{p}}$, as in the model with $j = 0$ at T .

If we have analogous functions $X(\theta)$ and $Y(\theta)$ satisfying $X(\mathbf{p}, \mathbf{r}) = X(\mathbf{r}) = Y(2\mathbf{r})$ then for their averages hold equation

$$\langle X(T) \rangle_{C, j=0} = \frac{1}{Z^{[0]}(T)} \int_{C'} \mathcal{D}\mathbf{r} 2^n Y(2\mathbf{r}) e^{-\frac{H^{[1]}(2\mathbf{r})}{4T}} = \frac{1}{Z^{[1]}(4T)} \int_C \mathcal{D}\theta Y(\theta) e^{-\frac{H^{[1]}(\theta)}{4T}} = \langle Y(4T) \rangle_{C, j=1}. \quad (1.14)$$

1.2.2 Similarity between J_1 and $-J_1$.

We consider $J_1 > 0$. Like in the previous subsection, we denote with an upper index the sign in front of J_1 ,

$$H^+ = - \sum_{\langle kl \rangle} [J_1 \cos(\theta_k - \theta_l) + J_2 \cos 2(\theta_k - \theta_l)], \quad (1.15)$$

$$H^- = - \sum_{\langle kl \rangle} [-J_1 \cos(\theta_k - \theta_l) + J_2 \cos 2(\theta_k - \theta_l)]. \quad (1.16)$$

We define the transformation $t : C \rightarrow C$ as following: Let $[x, y]$ be the coordinates of a spin in our square $N \times N$ lattice. Then we will change the angle of all spins with odd $(x + y)$ by π .⁶ It is not surprising that

$$H^+[t(\theta)] = H^-[\theta]. \quad (1.17)$$

The statistical sum $Z^+(T)$ is the same as $Z^-(T)$, because⁷

$$Z^+(T) = \int_C \mathcal{D}\theta e^{-\frac{H^+(\theta)}{T}} = \int_C \mathcal{D}\theta e^{-\frac{H^+[t(\theta)]}{T}} = \int_C \mathcal{D}\theta e^{-\frac{H^-(\theta)}{T}} = Z^-(T). \quad (1.18)$$

For the probabilities we get

$$p^+[t(\theta), T] = p^-[\theta, T], \quad (1.19)$$

and we can conclude that the phases of the model with J_1 must be in a one-to-one relation with the phases of the model with $-J_1$.⁸

1.2.3 Expectations

For $j = 1$, our model is identical to the usual XY model that has a ‘‘quasi’’-magnetic low-temperature phase (which will be referred to shortly as ‘‘magnet’’) and a disordered paramagnetic high-temperature phase (‘‘paramagnet’’). The phase transition at $T_C(j = 1)$ between the 2 phases is of the KT type.

For $j = 0$ the situation is almost the same (see Sec.1.2.1), only the low-temperature phase consists of spins with random orientations and the phase transition is result of unbinding of pairs consisting of a half-vortex and an anti-half-vortex. Half-vortices are excitations analogous to vortices in respect to the transformation Eq.(1.12). The low-temperature ordered phase with random spin orientation will be referred to as the nematic phase. The phase transition at $T_C(j = 0) = \frac{1}{4}T_C(j = 1)$ is of the KT type.

The aim of this thesis is to prove or disprove following hypotheses:

For small j , the dominant term in the Hamiltonian Eq.(1.3) is J_2 . For sufficiently small j we may sketch a gedanken experiment: at zero temperature the configuration is in the ground state, all spins are uniformly directed and oriented. If we heat up the configuration, there should exist a (low) temperature $T_1(j)$, at which the thermal fluctuations are of the same order as J_1 . At temperatures above $T_1(j)$ the spins became free in orientation (ruled by the J_1 -interaction), but they remain bound concerning their direction (ruled by the dominant J_2 -interaction) – the system undergoes a phase transition from the magnetic phase into the nematic phase. By further heating up we come to the temperature $T_2(j) \sim T_C(j = 0)$, at which the KT phase transition between the nematic and the paramagnetic phase due to half-vortex pair unbinding (as for $j = 0$) occurs.

⁶Every spin with odd $(x + y)$ has neighbours with even $(x + y)$ and vice versa.

⁷The Jacobian of the transformation t is 1.

⁸For example, if the model with J_1 at temperature T is in the ferromagnetic phase (or the paramagnetic, or the nematic), then the model with $-J_1$ at the same temperature T is in the antiferromagnetic phase (or the paramagnetic, or the nematic phase).

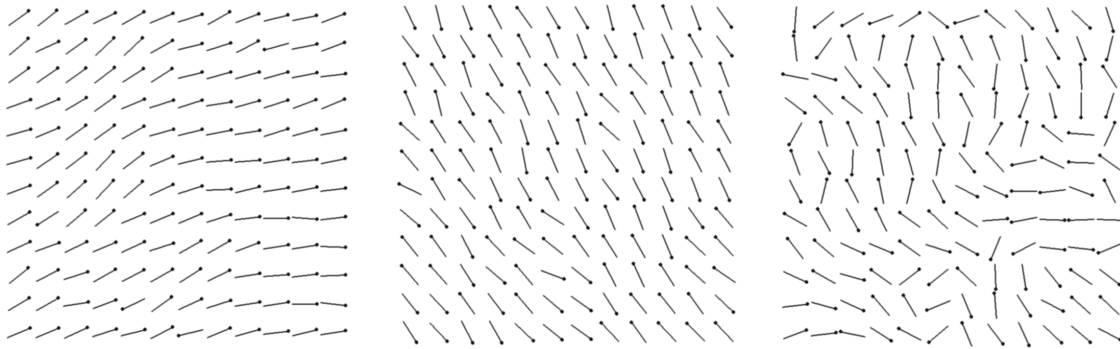


Figure 1.1: Typical spin configurations in the magnetic (left), the nematic (in the middle) and the paramagnetic (right) phase.

The phase transition at T_1 between the magnetic and nematic phases resembles the Ising phase transition.⁹ It is known that the phase transition for the Ising model defined by the Hamiltonian $H_{\text{Ising}} = -K \sum_{\langle kl \rangle} S_k S_l$, where $S_k = \pm 1$ and the coupling constant K is positive (ferromagnet), occurs at $T_{\text{Ising}} = \frac{2K}{\ln(1+\sqrt{2})}$. Therefore we may estimate that the phase transition between the magnetic and the nematic phase for our problem occurs at

$$T_1(j) \approx \frac{2jJ}{\ln(1+\sqrt{2})}. \quad (1.20)$$

Concluding, for values of j such that $T_1(j) < T_2(j)$ we should find 3 phases (the low-temperature magnetic phase, the intermediate-temperature nematic phase and the high-temperature paramagnetic phase) and 2 phase transitions (of the Ising type between the magnetic and the nematic phase, and of the KT type between the nematic phase and the paramagnet).

For j that do not satisfy the condition $T_1(j) < T_2(j)$ it might be expected that there exist only 2 phases: the magnet and the paramagnet, separated by the KT phase transition due to vortex unbinding.

⁹A similar Ising-like phase transition between “the nematic and almost-tetratic phase” is presented in [4].

Chapter 2

KT phase transition

2.1 The KT magnetic-paramagnetic phase transition

In this section we will derive the Kosterlitz-Thouless (KT) equation [2] for the magnetic-paramagnetic phase transition in the modified XY model. We claim that at the magnetic-paramagnetic phase transition the half-vortices do not play a role because the unbinding of them costs extra free energy of domain walls stretched between the half-vortex and anti-half-vortex (see Fig.2.1), which scales linearly with the distance between them. A free half-vortex in the paramagnetic phase at temperature T just above the magnetic-paramagnetic phase transition would have an infinitely long domain wall. Since in the magnetic phase the domain walls are energetically unfavorable, they would be also in the paramagnetic phase at temperature close to the phase transition. Thus, a free half-vortex would have linearly infinite free energy – which implies that free half-vortices are at the magnetic-paramagnetic phase transition not present.

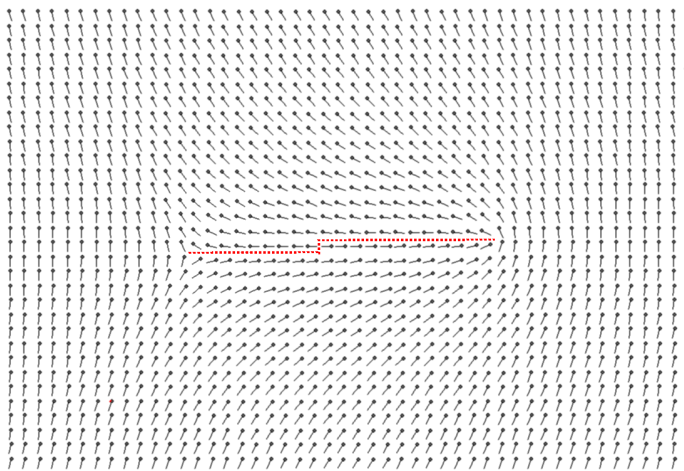


Figure 2.1: Configuration with a half-vortex (right) and an anti-half-vortex (left) “connected” with a domain wall (dotted segment line) for $j > 0$.

We will assume that the KT phase transition occurs only because of vortex pair unbinding. We will analyse the continuous model Eq.(1.6). We will inspect the problem far from boundaries, therefore we may assume periodic boundary conditions of a large square lattice, $\square_A = [-A, A] \times [-A, A]$ with sufficiently large $A > 0$. In order to minimize the energy we have to find the extrema of the functional $F[\theta(\mathbf{r})] = \int d^2r [\nabla\theta(\mathbf{r})]^2$. The extrema have to satisfy the *Laplace equation*¹

$$\Delta\theta(\mathbf{r}) = 0. \tag{2.1}$$

¹Our problem is therefore equivalent to the 2D electrostatics without charges.

The *Laplace equation* is solved by harmonic functions. A harmonic function $u(x, y)$ is smooth and if we add to it i times its harmonic conjugate function $\tilde{u}(x, y)$, we obtain a holomorphic complex function $u + i\tilde{u}$. The *Cauchy-Riemann equations* holds for them,

$$\frac{\partial u}{\partial x} = \frac{\partial \tilde{u}}{\partial y}, \quad \frac{\partial u}{\partial y} = -\frac{\partial \tilde{u}}{\partial x}. \quad (2.2)$$

Therefore both, the function u and the function \tilde{u} , are solutions of our variational problem. Moreover, the solutions have the same energy.

2.1.1 Vorticity

We will define a new quantity, the vorticity of a simply connected subset S of \square_A

$$V_\theta(S) = \frac{1}{2\pi} \oint_{\partial S} d\theta = \frac{1}{2\pi} \oint_{\partial S} \mathbf{dr} \cdot \nabla\theta, \quad (2.3)$$

where the contour integral is taken, as always in this paper, counter-clockwise.

2.1.2 Spin-wave solution

Functions that are solutions of *Laplace equation* in the whole region \square_A are smooth in \square_A . This type of solution we will call the spin-wave solution and denote it by ψ . It is clear that the harmonic conjugate function of a spin-wave solution is also a spin wave solution. We will introduce the differential operator $\nabla_\perp \equiv \partial_y \hat{\mathbf{e}}_1 - \partial_x \hat{\mathbf{e}}_2$ that applied on a continuously differentiable function u gives the vector ∇u rotated by $-\frac{\pi}{2}$ with a useful property

$$\nabla u = \nabla_\perp \tilde{u}, \quad \nabla_\perp u = -\nabla \tilde{u}. \quad (2.4)$$

The vorticity of a spin-wave solution for an arbitrary simply connected subset S is 0. We will prove that using the divergence theorem as follows

$$\oint_{\partial S} \mathbf{dr} \cdot \nabla\psi = \oint_{\partial S} dl \mathbf{n} \cdot \nabla_\perp \psi = \int_S d^2r \nabla \cdot \nabla_\perp \psi = 0, \quad (2.5)$$

where the unit vector \mathbf{n} is perpendicular to the loop ∂S and is directed outwards from S ; the differential operator $\nabla \cdot \nabla_\perp \equiv \partial_{xy} - \partial_{yx}$ applied on a smooth function gives 0.

2.1.3 Vortex

We will assume that the configuration $\theta(\mathbf{r})$ is a superposition of a continuously differentiable (smooth) spin-wave solution ψ with vorticity equal 0 and vortices – elementary point excitations with non-zero vorticity – that produce the field ϕ . A single vortex i in the point \mathbf{r}_i with 'charge' $q_i \in \{\pm 1\}$ is described by²

$$\phi_i(\mathbf{r}) = q_i \arg[(x - x_i) + i(y - y_i)]. \quad (2.6)$$

A vortex with positive "charge" will be referred to simply as a vortex, and vortex with negative 'charge' will be referred to as an anti-vortex; see Fig.2.2. The discontinuity for $x < x_i, y = y_i$ is irrelevant because the original (anharmonic) Hamiltonian Eq.(1.3) does not "see" the phase difference 2π there. Therefore we can simply ignore this discontinuity. However, the point discontinuity at \mathbf{r}_i is relevant and in that point the *Laplace equation* is not satisfied – therefore the vortex is a point excitation.

The vortex configuration can be defined by the vortex density

$$\rho(\mathbf{r}) = \sum_i q_i \delta(\mathbf{r} - \mathbf{r}_i). \quad (2.7)$$

The phase field corresponding to this vortex density is then

$$\phi(\mathbf{r}) = \sum_i q_i \arg[(x - x_i) + i(y - y_i)]. \quad (2.8)$$

²Remember that the complex logarithm $\ln \frac{z}{d} = \ln \frac{r}{d} + i \arg z$ with a real parameter d is holomorphic for $z \neq 0$.

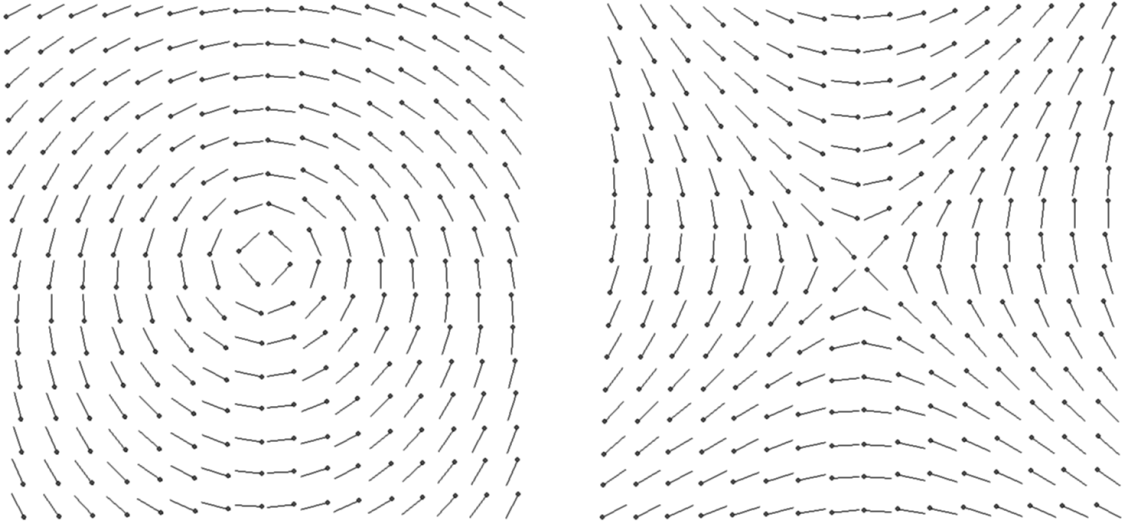


Figure 2.2: Examples of a single vortex (left) and an anti-vortex (right).

The harmonic conjugate field is

$$\tilde{\phi}(\mathbf{r}) = -\sum_i q_i \ln \frac{|\mathbf{r} - \mathbf{r}_i|}{d}. \quad (2.9)$$

Since $\Delta \left[\frac{1}{2\pi} \ln \frac{r}{d} \right] = \delta(\mathbf{r})$ in 2D, we may write for the harmonic conjugate field the following (Poisson) equation

$$\Delta \tilde{\phi} = -2\pi\rho. \quad (2.10)$$

The rotated gradient of ϕ is

$$\nabla_{\perp} \phi(\mathbf{r}) = -\nabla \tilde{\phi}(\mathbf{r}) = \sum_i q_i \frac{\mathbf{r} - \mathbf{r}_i}{|\mathbf{r} - \mathbf{r}_i|^2}. \quad (2.11)$$

Vorticity of a vortex configuration

The vorticity of a simply connected set $S \subset \square_A$ containing vortices indexed with i can be calculated as follows

$$\begin{aligned} V_{\phi}(S) &= \frac{1}{2\pi} \oint_{\partial S} d\mathbf{l} \cdot \nabla_{\perp} \phi = \frac{1}{2\pi} \int_{S'} d^2r \nabla \cdot \nabla_{\perp} \phi + \frac{1}{2\pi} \sum_i \oint_{\partial B(\mathbf{r}_i, \varepsilon)} d\mathbf{l} \cdot \nabla_{\perp} \phi, \\ &= 0 + \frac{1}{2\pi} \sum_i q_i \oint_{\partial B(\mathbf{r}_i, \varepsilon)} d\mathbf{l} \cdot \nabla \left[q_i \ln \frac{|\mathbf{r} - \mathbf{r}_i|}{d} - \tilde{\phi}_i \right] = \frac{1}{2\pi} \sum_i \oint_{\partial B(\mathbf{r}_i, \varepsilon)} d\mathbf{l} \left[\frac{q_i}{\varepsilon} - \mathbf{n} \cdot \nabla \tilde{\phi}_i \right] = \sum_i q_i, \end{aligned}$$

where $\tilde{\phi}_i(\mathbf{r}) \equiv -\sum_{j \neq i} q_j \ln \frac{|\mathbf{r} - \mathbf{r}_j|}{d}$ is the harmonic conjugate vortex field of all vortices in \square_A except for the vortex i ; ∂X stands for the boundary of set X . The useful trick was to apply the divergence theorem on a non-simply connected set $S' \equiv S \setminus \bigcup_i B(\mathbf{r}_i, \varepsilon)$ without open balls $B(\mathbf{r}_i, \varepsilon)$ around the vortices (see Fig.2.3) and to replace $\nabla_{\perp} u$ by $-\nabla \tilde{u}$. Thus we have found that the total vorticity is the sum of vortex charges inside S .

Energy of a vortex configuration

The energy of a single vortex located at the origin of a real (discrete) lattice is

$$H_{\text{vortex}} - H_{\text{ground}} \approx \frac{J}{2} \int_{\square_A \setminus B(\mathbf{0}, a')} d^2r (\nabla \phi)^2 \approx \pi J \int_{a'}^A \frac{dr}{r} \approx \pi J \ln \frac{A}{a'}, \quad (2.12)$$

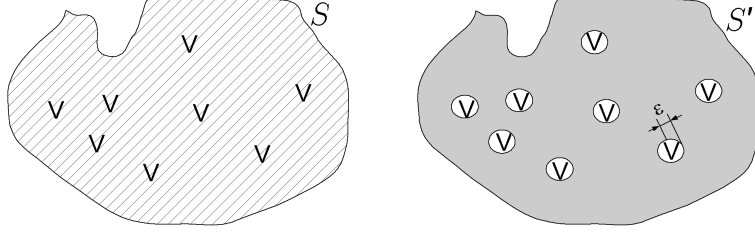


Figure 2.3: Left: A simply connected set S (hatched) containing vortices (displayed as “V”). Right: The non-simply connected set $S' \equiv S \setminus \bigcup_i B(\mathbf{r}_i, \epsilon)$ is shown as the grey area.

where the $a' \sim a$ is a cutoff of the integral at the lower boundary. The entropy of a single vortex is $S \approx \ln \frac{\pi A^2}{a^2} \approx 2 \ln \frac{A}{a}$. This indicates that the presence of a single vortex will lower the free energy $F = E - TS$ of the system for temperatures $T_C \gtrsim \frac{\pi J}{2}$. Below T_C there should not exist any free vortices.³ That enables us to consider periodic boundary conditions - namely, the total vorticity of \square_A with periodic boundary conditions is zero and therefore the number of positive vortices in \square_A with periodic boundary conditions must be equal to the number of anti-vortices.

We are trying to make a low-temperature approximation and therefore we may consider that there are no free vortices, only pairs of them. The energy of N vortices may be calculated as follows

$$\begin{aligned}
H - H_{\text{ground}} &= \frac{J}{2} \int_{\square'_A} d^2r [\nabla \tilde{\phi}]^2 + NH_{\text{core}} = \frac{J}{2} \int_{\square'_A} d^2r [\nabla(\tilde{\phi} \nabla \tilde{\phi}) - \tilde{\phi} \Delta \tilde{\phi}] + NH_{\text{core}}, \\
&= \frac{J}{2} \oint_{\partial \square'_A} dl \mathbf{n} \cdot (\tilde{\phi} \nabla \tilde{\phi}) - \frac{J}{2} \sum_i \oint_{\partial B(\mathbf{r}_i, a')} dl \mathbf{n} \cdot (\tilde{\phi} \nabla \tilde{\phi}) - 0 + NH_{\text{core}}, \\
&= 0 - \frac{J}{2} \sum_i \int_0^{2\pi} a' d\alpha \left(\tilde{\phi}_i(\mathbf{r}_i + a' \mathbf{n}) - q_i \ln \frac{a'}{d} \right) \left[\mathbf{n} \cdot \nabla \tilde{\phi}_i(\mathbf{r}_i + a' \mathbf{n}) - \frac{q_i}{a'} \right] + NH_{\text{core}}, \\
&= \pi J \sum_i q_i \left[\tilde{\phi}_i(\mathbf{r}_i) - q_i \ln \frac{a'}{d} \right] + NH_{\text{core}} = -\pi J \sum_{i \neq j} q_i q_j \ln \frac{r_{ij}}{d} + N\mu,
\end{aligned}$$

where we have denoted the integral $\int_{B(\mathbf{r}_i, a')} d^2r [\nabla \tilde{\phi}]^2$ of the energy of the core of a vortex or an anti-vortex as H_{core} . This term is within the continuous theory not well defined, but it is obvious that the term is the same for a vortex as well for an anti-vortex. The value of H_{core} contributes to the chemical potential μ of a single vortex. We have assumed that the value of $\tilde{\phi}_i(\mathbf{r}_i + a' \mathbf{n})$ has a sufficiently small variation in the neighbourhood of \mathbf{r}_i ; \square'_A denotes $\square_A \setminus \bigcup_i B(\mathbf{r}_i, a')$ and we have used that

- $\Delta \tilde{\phi} = 0$ everywhere in $\square_A \setminus \bigcup_i B(\mathbf{r}_i, a')$,
- $\oint_{\partial \square'_A} dl \mathbf{n} \cdot (\tilde{\phi} \nabla \tilde{\phi}) = 0$ because of periodic boundary conditions, since $\tilde{\phi}(\mathbf{r} + 2A \hat{\mathbf{e}}_x) = \tilde{\phi}(\mathbf{r})$ and $\nabla \tilde{\phi}(\mathbf{r} + 2A \hat{\mathbf{e}}_x) = \nabla \tilde{\phi}(\mathbf{r})$, and for y -direction similarly, but the vector \mathbf{n} directs always outwards of \square_A .

We may choose the constant d freely, so we set $d = a$. Then, the value of the chemical potential μ may be estimated for an isolated pair vortex-anti-vortex at the distance of lattice spacing a . We may place the vortex into a centre of an arbitrary square of lattice points and the anti-vortex into the centre of a square next to it. In case we place the vortex to $(-\frac{a}{2}, 0)$ and the anti-vortex to $(\frac{a}{2}, 0)$, then the chemical potential is given by

$$2\mu = J \sum_{\langle kl \rangle} \left[j + \frac{1-j}{4} - e(\theta_k - \theta_l) \right].$$

The precise value⁴ of μ may be calculated numerically by taking the sum over the nearby lattice points and

³The increase of the free energy due to a free vortex on a realistic lattice is huge, as $\frac{A}{a^2} \gg 1$.

⁴The drawback of this calculation is that on a real discrete lattice we should solve instead of the Laplace equation $\Delta \theta = 0$ (which assumed harmonic approximation) an array of (anharmonic) equations $\frac{\partial E_k}{\partial \theta_k} = \frac{1}{2} \sum_{\langle kl \rangle} e'(\theta_k - \theta_l) = 0$.

approximating the rest by an integral. The phase configuration is

$$\theta = \arg \left[\left(x + \frac{a}{2} \right) + iy \right] - \arg \left[\left(x - \frac{a}{2} \right) + iy \right],$$

$$\tilde{\theta} = -\frac{1}{2} \ln \frac{\left(x + \frac{a}{2} \right)^2 + y^2}{a} + \frac{1}{2} \ln \frac{\left(x - \frac{a}{2} \right)^2 + y^2}{a}$$

and corresponding term needed in integral is $[\nabla\theta]^2 = [\nabla\tilde{\theta}]^2 \approx \frac{a^2}{r^4}$ to the second order in the vortex distance a . Therefore, the energy of a vortex–anti-vortex pair may be calculated as follows

$$2\mu = J \sum_{\substack{\langle kl \rangle \\ |\mathbf{r}_k|, |\mathbf{r}_l| < R}} \left[j + \frac{1-j}{4} - e(\theta_k - \theta_l) \right] + \frac{J}{2} \int_R^\infty 2\pi r \, dr \frac{a^2}{r^4}.$$

The estimated value for $j = 1$ is $\mu = 3.311 J$.

2.1.4 Independence of spin waves and vortices

The continuously differentiable (smooth) spin-wave solution ψ is not a point of our study. We have to show that it is possible to study the vortex solution apart from spin waves – i.e. that the vortex solution and the spin-wave solution are independent, which means that the cross-term in energy vanishes:

$$\begin{aligned} \int_{\square_A} d^2r \, \nabla\psi \cdot \nabla\phi &= \int_{\square_A} d^2r \, \nabla\tilde{\psi} \cdot \nabla\tilde{\phi} = \int_{\square_A \setminus \bigcup_i B(\mathbf{r}_i, \varepsilon)} d^2r \, \left[\nabla \left(\tilde{\phi} \nabla\tilde{\psi} \right) - \Delta\tilde{\psi} \tilde{\phi} \right] + \sum_i \int_{B(\mathbf{r}_i, \varepsilon)} d^2r \, \nabla\tilde{\psi} \cdot \nabla\tilde{\phi}, \\ &= \oint_{\partial\square_A} dl \, \mathbf{n} \cdot \left(\tilde{\phi} \nabla\tilde{\psi} \right) - \sum_i \left[\nabla\tilde{\psi}(\mathbf{r}_i) \cdot \oint_{\partial B(\mathbf{r}_i, \varepsilon)} dl \, \tilde{\phi} \mathbf{n} \right] + \sum_i \left[\nabla\tilde{\psi}(\mathbf{r}_i) \cdot \int_{B(\mathbf{r}_i, \varepsilon)} d^2r \, \nabla\tilde{\phi} \right] = 0. \end{aligned}$$

All terms are zero:

- the first term: due to the periodic boundary conditions,
- the first sum is zero, because each integral is zero,

$$\left| \oint_{\partial B(\mathbf{r}_i, \varepsilon)} dl \, \tilde{\phi} \mathbf{n} \right| \leq \oint_{\partial B(\mathbf{r}_i, \varepsilon)} dl \, \left(\ln \frac{\varepsilon}{d} + \tilde{\phi}_i \right) \xrightarrow{\varepsilon \rightarrow 0^+} 0.$$

- the second sum is zero, because each integral is zero,

$$\left| \int_{B(\mathbf{r}_i, \varepsilon)} d^2r \, \nabla\tilde{\phi} \right| \leq \left| \int_{B(\mathbf{r}_i, \varepsilon)} d^2r \, \nabla\tilde{\phi}_i \right| + |q_i| \int_0^\varepsilon \frac{2\pi r \, dr}{r} \xrightarrow{\varepsilon \rightarrow 0^+} 0.$$

2.1.5 2D electrostatics

We will assume a configuration with dilute bound vortex–anti-vortex pairs. A dipole moment \mathbf{p} of a vortex configuration is, as usual, $\mathbf{p} = \int \rho(\mathbf{r}) \, d^2\mathbf{r} = \sum_i q_i$. The energy of the configuration described by $\tilde{\phi}(\mathbf{r})$ is

$$H_0 = \pi J \sum_i q_i \tilde{\phi}_i + \mu \sum_i q_i^2.$$

Now imagine that we add a new pair (the vortex into \mathbf{r}_+ and the anti-vortex into \mathbf{r}_-) into this configuration far away from each present vortex or anti-vortex. The dipole moment of the pair is $\mathbf{p} = \mathbf{r}_+ - \mathbf{r}_-$.⁵ The energy of this new configuration will be

$$H = H_0 + 2\mu + 2\pi J \ln \frac{p}{a} + 2\pi J \left[\tilde{\phi}(\mathbf{r}_+) - \tilde{\phi}(\mathbf{r}_-) \right] = H_0 + 2\mu + 2\pi J \ln \frac{p}{a} - 2\pi J \mathbf{E} \cdot \mathbf{p},$$

where $\mathbf{E} = -\nabla\tilde{\phi}$ is the analogue to the electric intensity.

⁵In our case, $|\mathbf{p}|$ is the length of the pair.

The polarizability $\alpha(p)$ of a pair (in rotationally invariant systems) with dipole moment p is defined

$$\alpha(p) = \lim_{E \rightarrow 0^+} \frac{\langle p(p) \rangle}{E} = \lim_{E \rightarrow 0^+} \frac{p \int_0^{2\pi} d\vartheta \cos \vartheta \exp \frac{2\pi J E p \cos \vartheta}{T}}{E \int_0^{2\pi} d\vartheta \exp \frac{2\pi J E p \cos \vartheta}{T}} = \frac{\pi J p^2}{T}. \quad (2.13)$$

Note that α depends on the length p of the dipole.

If the concentration of pairs (number of pairs per area) is n , then the polarization density is $\mathbf{P} = n \langle \mathbf{p} \rangle$ and the susceptibility is $\chi = 2\pi J \lim_{E \rightarrow 0^+} \frac{P}{E}$. Since the polarizability depends on the length of the dipole, we should write more correctly for uniformly small \mathbf{E}

$$\mathbf{P} = \int_0^\infty dp n(p) \langle \mathbf{p}(p) \rangle = \frac{1}{2\pi J} \int_0^\infty dp \chi(p) \mathbf{E}, \quad (2.14)$$

where $n(p)$ is the density of concentration of pairs with dipole moment p .⁶ Combining with Eq.(2.13) we obtain

$$\frac{1}{2\pi J} \chi(p) = \alpha(p) n(p). \quad (2.15)$$

For the intensity along the x axis $\mathbf{E} = (E, 0)$ the induced vortex density from pairs with fixed x -component of the dipole moment \mathbf{p} is equal to

$$\rho(p_x) = \frac{-n_{p_x}(x+dx) l p_x + n_{p_x}(x) l p_x}{l dx} = -\frac{\partial P_{p_x}}{\partial x},$$

see Fig.2.4. For an arbitrary intensity \mathbf{E} and integrated over all p_x we get $\rho_{\text{ind}} = -\nabla \cdot \mathbf{P}$.

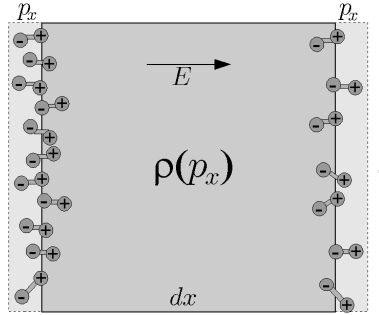


Figure 2.4: Visual help for deriving the formula for the induced vortex density.

The Poisson equation for the harmonic conjugate configuration Eq.(2.10) should be rewritten, if we take into account the polarization, as

$$\Delta \tilde{\phi} = -2\pi(\rho - \nabla \cdot \mathbf{P}), \quad \text{or} \quad \nabla \cdot (\mathbf{E} + 2\pi \mathbf{P}) = \nabla \cdot (\varepsilon \mathbf{E}) = 2\pi \rho. \quad (2.16)$$

2.2 KT equations

The dielectric function can be expressed using relations Eq.(2.14) and Eq.(2.15) as

$$\varepsilon = 1 + 2\pi \int dp \alpha(p) n(p), \quad (2.17)$$

where we have to be careful about the integration area. Namely, the dielectric function at small distances will not be affected by the pairs with a large dipole moment. More correctly, we have to introduce the dielectric function as a function of distance⁷

$$\varepsilon(r) = 1 + 2\pi \int_a^r dp \alpha(p) n(p). \quad (2.18)$$

⁶Thus $n(p) dp$ is the concentration of pairs with dipole moment from interval $[p, p + dp]$.

⁷The equation for the dielectric function $\varepsilon(r)$ is clearly not precise, because the upper boundary of the integral is only of the same order like r , it does not have to be exactly r .

The density of concentration $n(p)$ of pairs with the dipole moment p on a lattice $N \times N$ with spacing a is

$$n(p) dp = \frac{1}{(Na)^2} \frac{2\pi p dp}{a^2} e^{-V(p)/T}, \quad (2.19)$$

where $V(p)$ is the energy of the pair at distance p .

The energy of a vortex-anti-vortex pair in an empty (concerning other vortices) lattice is $V(r) = 2\mu + 2\pi J \ln \frac{r}{a}$. The energy of a pair in a polarisable (containing other vortices) medium is

$$V(r) = 2\mu + 2\pi J \int_a^r \frac{dr'}{r' \varepsilon(r')}, \quad (2.20)$$

where $\frac{2\pi J}{r' \varepsilon(r')}$ is the force between the vortex and the anti-vortex in polarisable medium.

Altogether, we have a system of 2 integral equations

$$\varepsilon(r) = 1 + \frac{4\pi^3 J}{a^4 T} \int_a^r dr' r'^3 e^{-\frac{V(r')}{T}}, \quad V(r) = 2\mu + 2\pi J \int_a^r \frac{dr'}{r' \varepsilon(r')}. \quad (2.21)$$

We will continue rewriting the above system following the [5]. We define

$$\varepsilon(r) \equiv \frac{K_0}{K(r)}, \quad \text{where } K_0 \equiv \frac{J}{T}, \quad (2.22)$$

$$U(r) \ln \frac{r}{a} \equiv \int_a^r \frac{K(r') dr'}{r'}, \quad (2.23)$$

$$y(r) \equiv y_0 \left(\frac{r}{a}\right)^{2-\pi U(r)}, \quad \text{where } y_0 \equiv e^{-\frac{\mu}{T}}. \quad (2.24)$$

Then it is possible to write the system in the form

$$y^2(r) = y_0^2 \left(\frac{r}{a}\right)^{4-2\pi U(r)}, \quad \frac{1}{K(r)} = \frac{1}{K_0} + 4\pi^3 \int_a^r \frac{dr'}{r'} y^2(r'), \quad (2.25)$$

or in the differential form

$$\frac{dK^{-1}(r)}{dr} = 4\pi^3 \frac{y^2(r)}{r}, \quad \frac{dy(r)}{dr} = \frac{2 - \pi K(r)}{r} y(r), \quad (2.26)$$

or, using the substitution $s \equiv \ln \frac{r}{a}$,

$$\frac{dK^{-1}(s)}{ds} = 4\pi^3 y^2(s), \quad \frac{dy(s)}{ds} = [2 - \pi K(s)] y(s), \quad (2.27)$$

with initial conditions

$$K(s=0) = K_0 = \frac{J}{T}, \quad y(s=0) = y_0 = e^{-\frac{\mu}{T}}. \quad (2.28)$$

The last form of the system of equations reveals that it has a fixed point for $K = \frac{2}{\pi}$, $y = 0$. We see that K is non-increasing function. Therefore if $K(s_0) = \frac{2}{\pi} - r$ and $r > 0$ for any s_0 , then $y(s)$ will grow faster then exponentially with s for $s > s_0$, and $K(\infty) = 0$; $K \xrightarrow{s \rightarrow \infty} 0$ means that the force between a vortex and an anti-vortex at large distance vanishes; thus the vortices may become free. On the other hand, $K(\infty) > 0$ means that the force between a vortex and an anti-vortex does not vanish even at large distances, thus the vortices are then (tightly) bound. Thus, the KT equations predict an universal jump $\frac{2T}{\pi}$ of K . The 2 basic types of solutions of equations Eq.(2.27) and the critical solution are shown in Fig.2.5.

In the neighbourhood of the fixed point, we may find asymptotic solution. If $K(s) = \frac{2}{\pi} + z(s)$ and $z(s_0) \ll \frac{2}{\pi}$ then $K^{-1} \approx \frac{\pi}{2} - \frac{\pi^2}{4} z$ and we get equations

$$z' = -16\pi y^2, \quad y' = -\pi z y. \quad (2.29)$$

We make ansatz $z = A s^\alpha$, $y = B s^\beta$. The obtained asymptotic solution is

$$K(s) = \frac{2}{\pi} + \frac{1}{\pi s} = \frac{2}{\pi} \left[1 + \frac{1}{2s}\right], \quad y = \frac{1}{4\pi s}. \quad (2.30)$$

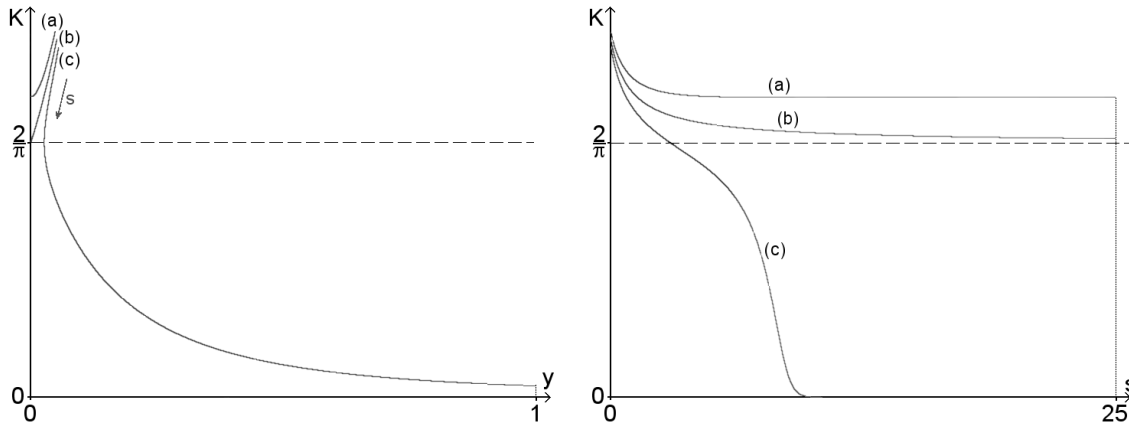


Figure 2.5: Numerical solution of the system of differential equations Eq.(2.27) with initial conditions $K(s=0) \equiv K_0 = \frac{J}{T}$ and $y(s=0) \equiv y_0 = e^{-\mu/T} = e^{-\mu K_0/J}$ (see Eq.(2.28)); the value of the chemical potential was taken for $j=1$, namely $\mu = 3.311 J$; the lines (a), (b) and (c) correspond to $K_0 = \frac{2}{\pi} + 0.23942$, $K_0 = \frac{2}{\pi} + 0.25942$ and $K_0 = \frac{2}{\pi} + 0.27942$, respectively. Left: The numerical solution in the plane K, y ; the arrow displays the evolution with the increasing s . Right: The numerical solution K as a function of s .

2.3 The KT nematic-paramagnetic phase transition

In the previous section we stated that half-vortices may unbind only at the transition between the nematic and the paramagnetic phase, because in the nematic phase the domain walls (which are stretched between the unbinding half-vortex and anti-half-vortex) are already present and therefore do not cost any additional free energy. As will be shown, the total energy of a free half-vortex is quarter of the total energy of a free vortex. That gives us argument why not to take the vortices at the nematic-paramagnetic phase transition into account.⁸

Therefore, we may assume that the KT phase transition occurs due to half-vortex unbinding. We revise the previous section in order to derive the KT equations for half-vortex pair unbinding. The changes are following:

- The ansatz for vortex configurations Eq.(2.6) remains, but possible charges for half-vortices (see Fig.2.6) are $q = \pm \frac{1}{2}$.⁹ The vortex density, the phase field and the harmonic conjugate have the same form. The Poisson equation Eq.(2.10) remains without changes, too.
- The energy of a free half-vortex is approximately

$$H_{\text{vortex}} - H_{\text{ground}} \approx \frac{J}{2} \int_{\square_A \setminus B(0, a')} d^2r (\nabla\phi)^2 \approx \frac{\pi J}{4} \int_{a'}^A \frac{dr}{r} \approx \frac{\pi J}{4} \ln \frac{A}{a'}, \quad (2.31)$$

which is 4-times less than the energy of a vortex. That explains why it is possible to neglect the effect of vortices at the phase transition between the nematic and the paramagnetic phase.

- Since the conjugate field does not change its form, the energy of a vortex solution will not change, too. The chemical potential μ does depend explicitly on j , as it was in the previous section. The proof of the independence of half-vortex solution on spinwaves might follow the proof of independence of vortex solution on spinwaves from the previous section.
- In the 2D electrostatics is the magnitude of dipole moment of a half-vortex–anti-half-vortex pair $|\mathbf{p}|$ half of the length of the pair. The energy of a dipole pair in the vortex configuration $-2\pi J \mathbf{E} \cdot \mathbf{p}$ remains valid. The polarizability as a function of distance r will be multiplied with the factor $\frac{1}{4}$,

$$\alpha(r) = \frac{\pi J r^2}{4T}. \quad (2.32)$$

⁸The argument is the same as why is in the usual XY model the effect of the double-vortices negligible; where a double-vortex has vorticity $\pm 4\pi$.

⁹For smoothness of the half-vortex solution out of their centers \mathbf{r}_i it is needed that the phase difference π is irrelevant in the Hamiltonian. This is true in the nematic phase.

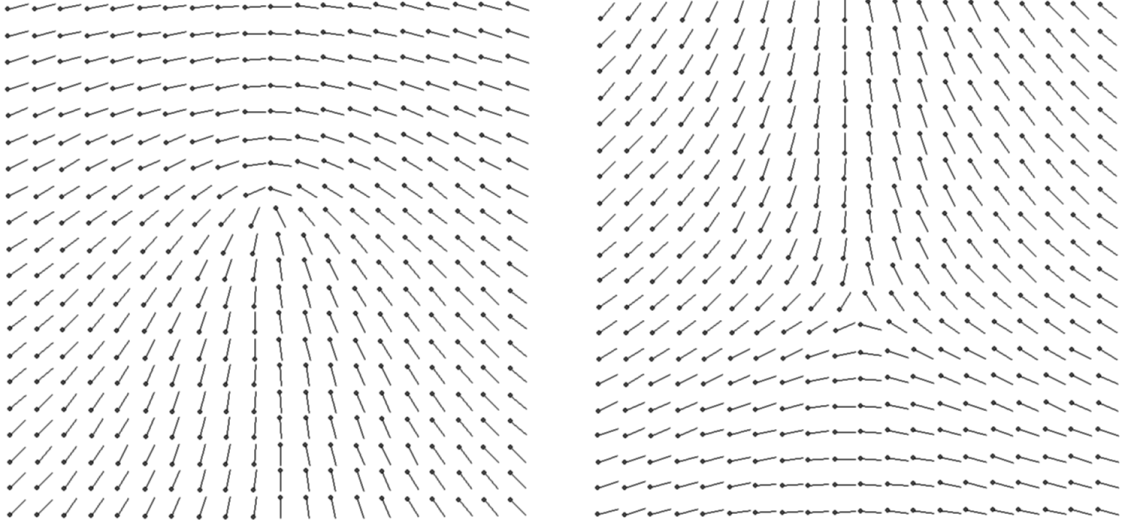


Figure 2.6: Examples of a single half-vortex (left) and an anti-half-vortex (right) for $j > 0$; in the model with $j = 0$ is the orientation of spins random.

The concentration $n(r) dr$ as a function of distance remains the same. The KT equations are

$$\varepsilon(r) = 1 + \frac{\pi^3 J}{a^4 T} \int_a^r dr' r'^3 e^{-\frac{V(r')}{T}}, \quad V(r) = \frac{\mu}{2} + \frac{\pi J}{2} \int_a^r \frac{dr'}{r' \varepsilon(r')}. \quad (2.33)$$

We define

$$\varepsilon(r) \equiv \frac{K_0}{K(r)}, \quad \text{where } K_0 \equiv \frac{J}{T}, \quad (2.34)$$

$$U(r) \ln \frac{r}{a} \equiv \int_a^r \frac{K(r')}{r'} dr', \quad (2.35)$$

$$y(r) \equiv y_0 \left(\frac{r}{a} \right)^{2 - \frac{\pi U(r)}{4}}, \quad \text{where } y_0 \equiv e^{-\frac{\mu}{4T}}. \quad (2.36)$$

and after the substitution $s = \ln \frac{r}{a}$ we obtain equations

$$\frac{dK^{-1}(s)}{ds} = \pi^3 y^2(s), \quad \frac{dy(s)}{ds} = \left[2 - \frac{\pi}{4} K(s) \right] y(s), \quad (2.37)$$

with initial conditions

$$K(s=0) = K_0 = \frac{J}{T}, \quad y(s=0) = y_0 = e^{-\frac{\mu}{4T}}. \quad (2.38)$$

- If we analyze the system of equations Eq.(2.37) we see that the universal jump is in this case $\frac{8T}{\pi}$. From the analysis near the fixed point we get the asymptotic solution

$$K(s) = \frac{8}{\pi} \left[1 + \frac{1}{2s} \right]. \quad (2.39)$$

2.4 Renormalization of J due to anharmonicity

The low-temperature harmonic approximation of the Hamiltonian Eq.(1.4) is

$$H_0 = \frac{J}{2} \sum_{\langle kl \rangle} (\theta_k - \theta_l)^2. \quad (2.40)$$

With gradient \mathbf{q} of externally imposed global twist in the limit $q \equiv |\mathbf{q}| \rightarrow 0$ we study the effects of long waves that are responsible for the long-range disorder. The extended low-temperature harmonic approximation of Hamiltonian is then¹⁰

$$H_0(q) = \frac{J}{2} \sum_{\langle kl \rangle} (\theta_k - \theta_l + \mathbf{q} \cdot \mathbf{r}_{kl})^2 = \frac{1}{2} J N^2 a^2 q^2 + H_0, \quad (2.41)$$

where the mixed term is zero because of periodic boundary conditions of the configuration θ :

$$J \sum_{\langle kl \rangle} (\theta_k - \theta_l) \mathbf{q} \cdot \mathbf{r}_{kl} = J q_x a \sum_{\text{rows}} \underbrace{\sum_{\text{columns}} (\theta_k - \theta_l)}_0 + J q_y a \sum_{\text{columns}} \underbrace{\sum_{\text{rows}} (\theta_k - \theta_l)}_0 = 0.$$

The free energy of the harmonic approximation is

$$F_0(q) = -T \ln \int \mathcal{D}\theta e^{-\frac{H_0(q)}{T}} = F_0(0) + \frac{1}{2} J N^2 a^2 q^2. \quad (2.42)$$

The extended (original, anharmonic) Hamiltonian is

$$H(q) = \sum_{\langle kl \rangle} [(J_1 + J_2) - J_1 \cos(\theta_k - \theta_l + \mathbf{q} \cdot \mathbf{r}_{kl}) - J_2 \cos 2(\theta_k - \theta_l + \mathbf{q} \cdot \mathbf{r}_{kl})]. \quad (2.43)$$

The free energy to the 1st order in $(H - H_0)/T$ is then

$$F = -T \ln \int \mathcal{D}\theta e^{-\frac{H(q)}{T}} = -T \ln \int \mathcal{D}\theta e^{-\frac{H_0(q)}{T}} \left(1 - \frac{H(q) - H_0(q)}{T} \right) = F_0(q) + \langle H(q) - H_0(q) \rangle_0, \quad (2.44)$$

where $\langle X \rangle_0$ is the thermal average of the quantity X according to H_0 ,¹¹

$$\langle X \rangle_0 = \frac{\int \mathcal{D}\theta X(\theta) e^{-\frac{H_0}{T}}}{\int \mathcal{D}\theta e^{-\frac{H_0}{T}}}. \quad (2.45)$$

Applying the equipartition theorem on the extended Hamiltonian approximation Eq.(2.41) we easily obtain¹²

$$\langle H_0 \rangle_0 = \frac{N^2 T}{2}, \quad \text{and} \quad \langle H_0(q) \rangle_0 = \frac{N^2 T}{2} + \frac{1}{2} J N^2 a^2 q^2. \quad (2.46)$$

We need to derive the relation for $\langle H(q) \rangle_0$,

$$\langle H(q) \rangle_0 = \sum_{\langle kl \rangle} [(J_1 + J_2) - J_1 \langle \cos(\theta_k - \theta_l) \rangle_0 \cos(\mathbf{q} \cdot \mathbf{r}_{kl}) - J_2 \langle \cos 2(\theta_k - \theta_l) \rangle_0 \cos(2\mathbf{q} \cdot \mathbf{r}_{kl})], \quad (2.47)$$

where the terms $\langle \sin(\theta_k - \theta_l) \rangle_0$, resp. $\langle \sin 2(\theta_k - \theta_l) \rangle_0$ are trivially 0 from the symmetry of bond energy e . From the spin-wave low-temperature theory we get $\langle \cos(\theta_k - \theta_l) \rangle_0 = 1 - \frac{T}{4J}$ to the 1st order in T , and $\langle \cos 2(\theta_k - \theta_l) \rangle_0 = 1 - \frac{T}{J}$. Inserting these relations into the last formula and using $J_1 + 4J_2 = J$, and $J_1 = jJ$ we obtain

$$\langle H(q) \rangle_0 = \frac{N^2 T}{2} + \frac{1}{2} J N^2 a^2 q^2 \left[1 - \frac{4 - 3j T}{4 J} \right] \quad (2.48)$$

Inserting Eq.(2.46) and Eq.(2.48) into Eq.(2.44) and reorganizing we get

$$F(q) = F(0) + \frac{1}{2} J N^2 a^2 q^2 \left(1 - \frac{4 - 3j T}{4 J} \right). \quad (2.49)$$

Analogical to the mechanical modulus in the mechanics of of continuum we may define the helicity modulus Υ of a square lattice with $n \equiv N^2$ sites and lattice constant a as

$$\Upsilon = \frac{1}{N^2 a^2} \left. \frac{\partial^2 F}{\partial q^2} \right|_{q=0}, \quad (2.50)$$

¹⁰The concept is that the solution θ satisfies periodic boundary conditions, but the externally imposed global twist \mathbf{q} appears in the Hamiltonian.

¹¹Note, that the thermal average of X according to $H_0(q)$ is the same as $\langle X \rangle_0$.

¹²It is also possible to verify the result within the spin-wave theory.

where F is the free energy of the lattice and $q = |\mathbf{q}|$ is the magnitude of gradient \mathbf{q} of externally imposed global twist [6].

The interpretation of the formula is that the coupling constant J is *effectively* renormalized in the presence of long-wave spin waves as follows,

$$J \mapsto J' \equiv J \left[1 - \left(1 - \frac{3j}{4} \right) \frac{T}{J} \right]. \quad (2.51)$$

Thus the Hamiltonian for continuous model Eq.(1.6) is in the presence of spin waves *effectively* equal to

$$H - H_{\text{ground}} = \frac{J'}{2} \int d^2r [\nabla\theta(\mathbf{r})]^2 \quad (2.52)$$

and that is the Hamiltonian for which we have to derive the KT equations.

2.5 Renormalization of J due to vortex unbinding

According to [7], the helicity modulus Υ defined in Eq.(2.50) is identical with the $K(r \rightarrow \infty)$ defined in Eq.(2.22),

$$\Upsilon(j, T) = K(j, T, r \rightarrow \infty). \quad (2.53)$$

Thus, we have 2 sources of J renormalization. Since the KT theory is harmonic, it is reasonable to renormalize the coupling J first due to the anharmonicity and then to use the renormalised J' as an input for the KT theory. Thus, the KT renormalization due to the vortex–anti-vortex pair unbinding¹³ involves solving the KT equations Eq.(2.27) with initial conditions

$$K(s=0) = K_0 = \frac{J'}{T}, \quad y(s=0) = y_0 = e^{-\frac{\mu'}{T}}, \quad (2.54)$$

where the μ' is the chemical potential computed with the the renormalized J' . However, for $j \neq 0, 1$ it remains unclear how to compute the contribution of the nearest neighbourhood since we do not know from the renormalization due to anharmonicity how is renormalized the J_1 -interaction and J_2 -interaction separately.

We have compared the twice renormalized J , firstly due to anharmonicity and secondly due to vortex–anti-vortex pair unbinding, for $j = 1$ with the Υ obtained from a Monte Carlo simulation; see Fig.2.7.

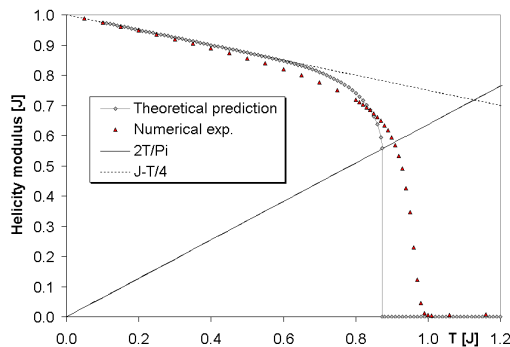


Figure 2.7: Comparison of the twice renormalized J as a function of T (called *Theoretical prediction*), i.e. $K(j = 1, T, r \sim 250 \gg 1)$, and the Υ resulting from numerical experiments to be described later (on a lattice with linear size $N = 256$); for $j = 1$. The line $\frac{2T}{\pi}$ shows the predicted universal jump of helicity. The dotted line $J - \frac{T}{4}$ is the renormalized J' due to anharmonicity.

¹³For half-vortex–anti-half-vortex pair unbinding similarly, only using the equations Eq.(2.37) and initial conditions Eq.(2.38).

Chapter 3

Monte Carlo simulation

The system of our interest is the lattice of $N \times N$ spins at a defined temperature. The probability distribution is given by the Boltzman distribution $p(\theta) = \frac{1}{Z} e^{-\frac{E(\theta)}{T}}$. An ideal algorithm that would compute averages of physical quantity x of the lattice at defined temperature should construct all possible states θ of the lattice, measure the quantity $x(\theta)$ and compute average $\langle x \rangle = \sum_{\theta} p(\theta) x(\theta)$. For most systems – and our lattice is no exception – this straightforward method is not executable, because the number of all states is huge or infinite.

A solution may be an randomized (Monte Carlo, shortly MC) algorithm that would construct randomly chosen configurations from the space of all possible states with relative probabilities in consensus with the Boltzman distribution, which means $\frac{p_a}{p_b} = e^{\frac{E_b - E_a}{T}}$ for any 2 states a and b . I will prove that an algorithm producing a chain of configurations with following properties will in limit of infinite number of steps generate states with appropriate relative probabilities:

- The algorithm generates next configuration randomly from the current state.
- The algorithm is ergodic, i.e. can reach any of all possible states of the physical system.
- The algorithm satisfies condition

$$p(b \rightarrow a) = e^{\frac{E_b - E_a}{T}} p(a \rightarrow b), \quad \forall a, b, \quad (3.1)$$

where $p(a \rightarrow b)$ is the probability of generating configuration b from a in a single step.

Proof follows [8]: The space of all possible configurations θ is in practice always finite.¹ I choose two arbitrary states a and b . Since the algorithm is ergodic, there must exist sequences $S[k]$ of states $a \equiv C_0 \rightarrow C_1 \rightarrow C_2 \rightarrow \dots \rightarrow C_k \equiv b$ for that $p(C_i \rightarrow C_{i+1}) > 0$ for $i = 0, 1, \dots, k-1$.² We choose the shortest sequence. If there are more sequences of the smallest length, then we choose arbitrarily any of them. We denote the energy differences, $\Delta E_i \equiv E_i - E_{i-1}$. The ratio Q'_{ba} of probability of changing state b into a according to the chosen sequence, and the probability of the reverse process is then

$$Q'_{ba} = \frac{p_{S[k]}(b \rightarrow a)}{p_{S[k]}(a \rightarrow b)} = \frac{\prod_{i=1}^k p(C_k \rightarrow C_{k-1})}{\prod_{i=1}^k p(C_{k-1} \rightarrow C_k)} = \prod_{i=1}^k \frac{p(C_k \rightarrow C_{k-1})}{p(C_{k-1} \rightarrow C_k)} = \prod_{i=1}^k \exp\left(\frac{\Delta E_i}{T}\right) = \exp\left(\frac{E_b - E_a}{T}\right).$$

The ratio Q'_{ba} does not depend on the chosen sequence $S[k]$. Therefore the ratio $Q_{ba} = \frac{p_k(b \rightarrow a)}{p_k(a \rightarrow b)}$ of probability of changing state b into a in an arbitrary sequence of length k , and the probability of the reverse process is the same, $e^{\frac{E_b - E_a}{T}}$.

Now, consider a large ensemble of systems. Let n_a be the number of systems of the ensemble in the state a . The net number of systems moving in k steps from the state a to b is

$$n_{a \rightarrow b}^{(k)} = n_a p_k(a \rightarrow b) - n_b p_k(b \rightarrow a) = \left[n_a - n_b e^{\frac{E_b - E_a}{T}} \right] p_k(a \rightarrow b). \quad (3.2)$$

¹Also our lattice of $N \times N$ spins is in the computer realization finite space.

²The condition Eq.(3.1) guarantees for such a sequence $S[k]$ that there is a non-zero probability of the reverse process.

We see that for the arbitrarily chosen states a and b , if $\frac{n_a}{n_b} < e^{\frac{E_b - E_a}{T}}$, on the average more systems move from state b to a . Thus the ensemble of systems must approach the canonical distribution. \square

In reality, the program does not generate every state. The convergence of the averages is also delicate. Usually, the simulation runs from an initial state that might be quite improbable. The time (number of necessary steps) to get into the highly probable configurations is called *thermalization time* and the measurements during this time are not included in the calculation of averages. We determine the thermalization time by measuring all interested quantities and by inspecting whether they are stabilized or not. There is another complication called ergodicity breaking, when there are more regions with highly probable states separated³ by regions with highly improbable states.

3.1 The Metropolis algorithm

The Metropolis algorithm [8] is a randomized algorithm that enables the simulation of thermal equilibrium of our lattice. Each step consists of

1. Choosing randomly one site k of the lattice.
2. Choosing randomly an angle $\alpha \in [0, \pi)$.
3. Calculating the energy difference $\Delta E = E^* - E$, where E denotes the actual energy and E^* stands for a configuration, in which the spin at site k is flipped around an axis defined by the angle α .⁴
4. If $\Delta E < 0$, then we accept the new configuration. Otherwise, we accept it with probability $\exp(-\frac{\Delta E}{T}) < 1$.

It is obvious that our algorithm is ergodic and that new configurations are generated randomly. We show that for the probability of changing state b into a in a single step and for the backwards process the condition Eq.(3.1) holds,⁵

$$\frac{p(b \rightarrow a)}{p(a \rightarrow b)} = \frac{P(k, \alpha) \exp(-\frac{H(\Delta E)\Delta E}{T})}{P(k, \alpha) \exp(-\frac{H(-\Delta E)\Delta E}{T})} = \exp\left(-\frac{[H(\Delta E) + H(-\Delta E)]\Delta E}{T}\right) = \exp\left(\frac{E_b - E_a}{T}\right),$$

where $P(k, \alpha)$ is the probability of choosing the site k and the angle α , and $H(x)$ is the Heaviside function.⁶

The length of the thermalization period depends on the lattice size, temperature T , coupling parameter j , as well as on the initial configuration. It is strongly recommended to thermalize gradually, otherwise it is much more probable that metastable configurations appear – the reason for that is that Metropolis' steps act only locally – the Metropolis algorithm is applicable also to the study of locally stable configurations.

3.2 The Wolff algorithm

The Wolff algorithm [9] flips whole clusters of spins. Its main benefits are quicker thermalization and shorter autocorrelation times. The random step scheme consists of these phases

1. Choosing randomly one site k of the lattice, we will call it the seed.
2. Choosing randomly an angle $\alpha \in [0, \pi)$.
3. Flipping the spin at the site k of the lattice around the axis α , that means $\theta_k^* = 2\alpha - \theta_k$.
4. Flip each unflipped neighbour i of the site k with probability $P(k, i)$ and repeat this procedure for the site i .

³Separated in terms of the algorithm step, i.e. the program cannot change configuration from one region with probable states into configuration of the another region with probable states directly, only “crossing” improbable regions. An example might be the Ising model simulated by Metropolis algorithm (see Sec.3.1) at low temperatures. There are 2 highly probable states (all spins up or down). The probability of flipping all spins by the algorithm is effectively zero. Thus the ergodicity is broken.

⁴The angle of the flipped spin is then $\theta_i^* = 2\alpha - \theta_i$. Note that the energy difference may arise only from changes of bond energies between the spin k and its neighbours.

⁵For configurations that differ in more than one spin it is trivial.

⁶The Heaviside function is defined by the formula $H(x) = \frac{1 + \text{sgn}(x)}{2}$.

The set of all flipped spins in a single step is called cluster. The probability of flipping a neighbour i of site k is

$$P(k, i) = 1 - \min \left\{ 1, \exp \left[\frac{e(\theta_k - \theta_i) - e(\theta_k^* - \theta_i)}{T} \right] \right\}, \quad (3.3)$$

where $e(\theta_k - \theta_l)$ is the energy of a single bond between spins k and l defined in Eq.(1.5).⁷

It is again obvious that the algorithm is ergodic and that it generates new configurations randomly. We have to prove that for any two configurations a and b the equation $p(b \rightarrow a) = e^{\frac{E_b - E_a}{T}} p(a \rightarrow b)$ is valid. We will do it in following 3 steps:

- First of all, we realize that the probability of choosing certain angle α is the same for the forward as for the backward process. The probability of choosing a particular seed is $\frac{1}{N^2}$.
- Secondly, we show that the ratio of the probability of flipping a certain cluster S that has grown from a particular seed site in an exactly defined way (r) around defined axis and probability of the reverse process⁸ is $\exp \frac{E - E^*}{T}$ where $E - E^*$ stands for minus energy difference of the configurations; E stands for the original energy of a and E^* is the energy of the state b with flipped cluster S .

We need to analyze the process of increasing the cluster. A spin may be added to the cluster visiting from 4 neighbours. We can not exclude that it will be added to the cluster after some unsuccessful attempts from other sides. We will assume that the algorithm is deterministic concerning the rules of visiting the neighbours. That guarantees that for growing the cluster in a defined way, we need to ask for the same probabilities $P(k, i)$. The probability of flipping a neighbour i of a flipped spin k in the forward process is

$$P_{forw}(k, i) = 1 - \min \left\{ 1, \exp \frac{e(\theta_k - \theta_i) - e(\theta_k^* - \theta_i)}{T} \right\}. \quad (3.4)$$

In the reverse process, the probability of flipping a neighbour $i \in S$ (i.e. from the cluster, flipped in forward process) of a spin k in the cluster (already twice flipped) is

$$P_{rev}(k, i) = 1 - \min \left\{ 1, \exp \frac{e(\theta_k^* - \theta_i^*) - e(\theta_k - \theta_i^*)}{T} \right\}. \quad (3.5)$$

Since $\theta_k^* - \theta_i^* = \theta_i - \theta_k$ and $(\theta_k^*)^* = \theta_k$ and $e(\theta_k - \theta_l) = e(\theta_l - \theta_k)$, we see that the probabilities Eq.(3.4) and Eq.(3.5) are the same.

The situation changes, when we look at the probability not to flip in the reverse process a neighbour i outside of the cluster (visiting from a already twice flipped spin inside of S)

$$1 - P_{rev}(k, i) = \min \left\{ 1, \exp \frac{e(\theta_k^* - \theta_i) - e(\theta_k - \theta_i)}{T} \right\}. \quad (3.6)$$

Altogether, we may write for the ratio of probabilities of flipping and deflipping the cluster S that has grown in the same way (r)

$$\begin{aligned} \frac{p_{forw}^{(r)}}{p_{rev}^{(r)}} &= \frac{\prod_{\langle ki \rangle, k \in S, i \notin S} [1 - P_{forw}(k, i)]}{\prod_{\langle ki \rangle, k \in S, i \notin S} [1 - P_{rev}(k, i)]} = \prod_{\langle ki \rangle, k \in S, i \notin S} \frac{\min \left\{ 1, \exp \frac{e(\theta_k^* - \theta_i^*) - e(\theta_k - \theta_i^*)}{T} \right\}}{\min \left\{ 1, \exp \frac{e(\theta_k^* - \theta_i) - e(\theta_k - \theta_i)}{T} \right\}}, \\ &= \prod_{\langle ki \rangle, k \in S, i \notin S} \exp \frac{e(\theta_k - \theta_i) - e(\theta_k - \theta_i^*)}{T} = \exp \left[-\frac{E^* - E}{T} \right], \end{aligned}$$

because the term $e(\theta_k - \theta_i) - e(\theta_k - \theta_i^*)$ is the minus energy change in bond between sites i and k and the energy of the configuration with flipped cluster S differs only in the bonds between spins inside of the cluster and spins outside of it. \square

⁷Note that the bond energy e is a symmetric function; it is important for appropriate functionality of this implementation of Wolff's algorithm.

⁸The reverse process does mean that the seed site is the same, the axis is the same and the way (r) of growing of the cluster is the same. The only difference is that we are flipping the state b instead of a .

- Lastly, we show that the ratio of probability of flipping certain cluster S in any possible way around defined axis and probability of the reverse process is $\exp \frac{E-E^*}{T}$. Because the ratio of flipping a cluster and deflipping the same cluster in the same way does not depend on the details of the growth of the cluster, we can formally write

$$\frac{p_{rev}}{p_{forw}} = \frac{\sum_r p_{rev}^{(r)}}{\sum_r p_{forw}^{(r)}} = \frac{\sum_r p_{forw}^{(r)} \exp \frac{E^*-E}{T}}{\sum_r p_{forw}^{(r)}} = \exp \frac{E^* - E}{T},$$

where the sum is over all possible ways (r) of growth of the specified cluster S . \square

An important difference between the Metropolis and the Wolff algorithm apart from time-efficiency is also the more variable step of the Wolff algorithm, which minimizes the possibility of ergodicity breaking.

3.3 Autocorrelation time and error of the mean

For each measurable quantity x we have a sequence $\{x_i\}_{i=1}^M$ of measured values and we may define the autocorrelation function

$$R_x(\tau) = \frac{1}{(M-\tau) s_x^2} \left[\sum_{i=1}^{M-\tau} x_i x_{i+\tau} - (M-\tau) \langle x \rangle_{[1, M-\tau]} \langle x \rangle_{[\tau+1, M]} \right], \quad (3.7)$$

where $\tau \in \mathbb{Z}_0^+$ and $\tau < M$. The denominator in the front ensures that $|R_x(\tau)| \leq 1$, since s_x is the sample standard deviation of the measurements of x ,

$$s_x^2 = \frac{1}{M} \sum_{i=1}^M x_i^2 - \langle x \rangle_{[1, M]}^2.$$

The notation $\langle x \rangle_{[i, j]}$ stands for the mean value of a sequence of measurements of x starting with index i and ending with j . If we denote $\Delta_i = x_i - \langle x \rangle_{[1, M-\tau]}$ and $\Delta'_i = x_i - \langle x \rangle_{[\tau+1, M]}$, then we obtain

$$R_x(\tau) = \frac{1}{(M-\tau) s_x^2} \sum_{i=1}^{M-\tau} \Delta_i \Delta'_{i+\tau}.$$

Even for $\frac{M}{\tau} \approx 100$ is the difference between $\langle x \rangle_{[1, M-\tau]}$ and $\langle x \rangle_{[1, M]}$ important and cannot be neglected.

We assume that the autocorrelation function is $R_x(\tau) = e^{-\tau/T}$; a real example of autocorrelation function is shown in the figure Fig.3.1. Then the average of the autocorrelation for all pairs of measured points is

$$\rho = \frac{2}{M(M-1)} \sum_{i=1}^{M-1} \sum_{j=i+1}^M R_x(j-i) \approx \frac{2T}{M},$$

where we considered $T \ll M$. According to [10], the standard deviation of the mean $\langle x \rangle \equiv \langle x \rangle_{[1, M]}$ is $s_{\langle x \rangle} = \sqrt{\frac{1+(M-1)\rho}{M(1-\rho)}} s_x \approx \sqrt{\frac{1+2T}{M}} s_x$.⁹

3.4 Measured observables

In our simulation we compute after every Q random steps¹⁰ these quantities

⁹Another simple argument might be following: 2 measurements with autocorrelation $R_x = 0.1$ might be considered as almost independent. The number of *effectively independent measurements* is then roughly $\frac{M}{\tau_x}$, where τ_x is the time for that $R_x(\tau_x) \approx 0.1$. Then, the standard error of the mean $\langle x \rangle$ is approximately $s_{\langle x \rangle} \approx \sqrt{\frac{\tau_x}{M}} s_x$.

¹⁰The value of Q is set appropriate to the autocorrelation times of the measured quantities.

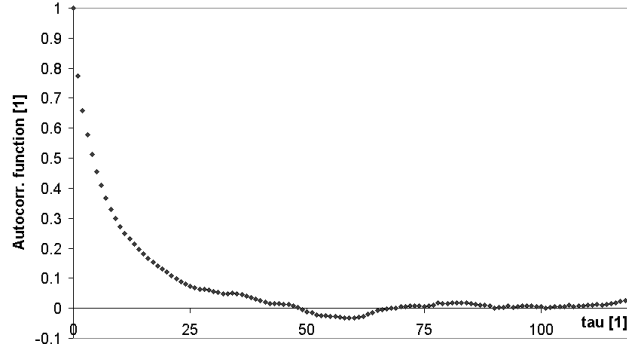


Figure 3.1: Plot of autocorrelation function $R_m(\tau)$ for the parameter m (see Sec.3.4). The data was obtained on the lattice 256×256 at temperature $T = 0.0442 J$ with 250 MC steps between each measurement. The numerical experiment was performed by the Wolff algorithm.

- *Energy*, '*derivative*' of energy and '*second derivative*' of energy:

$$E = -J \sum_{\langle kl \rangle} [j \cos(\theta_k - \theta_l) + j_2 \cos 2(\theta_k - \theta_l)], \quad (3.8)$$

$$E^{(1)} = J \sum_{\langle kl \rangle} [j \sin(\theta_k - \theta_l) + 2j_2 \sin 2(\theta_k - \theta_l)], \quad (3.9)$$

$$E^{(2)} = J \sum_{\langle kl \rangle} [j \cos(\theta_k - \theta_l) + 4j_2 \cos 2(\theta_k - \theta_l)], \quad \text{respectively.} \quad (3.10)$$

- *Magnetization* in direction x and y :

$$M_x = \sum_k \cos \theta_k, \quad \text{and} \quad M_y = \sum_k \sin \theta_k, \quad \text{respectively.} \quad (3.11)$$

- '*Nematic magnetization*' in direction x and y :

$$N_x = \sum_k \cos 2\theta_k, \quad \text{and} \quad N_y = \sum_k \sin 2\theta_k, \quad \text{respectively.} \quad (3.12)$$

- *Vorticity* V : the total number of vortices with positive charge per spin. Vortex detection is performed at each plaquette – an elementary square with 4 corner lattice sites – counting the angle differences in a defined way (anti-clockwise) around the square [11]. The angle differences have to lie within $(-\pi, \pi]$. The possible results of the sum of differences are 0 or $\pm 2\pi$; the result $\pm 2\pi$ is interpreted as a vortex, or an anti-vortex in the plaquette. The vorticity of a bigger area is simply the sum of the vorticities of its plaquettes. Since the whole lattice has periodic boundary conditions, we can conclude that the number of negative vortices must be the same as the number of the positive vortices. See Fig.3.2.
- *Half-vorticity* V_H : the total number of half-vortices with positive charge per spin. A half-vortex is for $j = 0$ analogue of the vortex for $j = 1$. It is detected using the same technique as vortex, the only difference is that we sum angle differences of unoriented lines instead of oriented 'arrows'.¹¹ Making use of the argument about similarity (see Sec.1.2.1) it can be easily shown that the average vorticity for $j = 1$ at temperature T is the same as the half-vorticity for $j = 0$ at temperature $\frac{T}{4}$. See Fig.3.2.
- *Walls* W : the total number of walls between pairs of spins per spin. We say that between a neighbouring pair of spins k, l there is a wall, if $|\theta_k - \theta_l| \geq \arccos \frac{j}{j-1}$, because the force between the spins acts then in the direction to make them opposite to each other.¹² See Fig.3.2.

¹¹The angle differences have to lie within $(-\frac{\pi}{2}, \frac{\pi}{2}]$. The sum around a plaquette is then 0 or $\pm\pi$. The result $\pm\pi$ is interpreted as a half-vortex with positive, or negative charge.

¹²For $j \geq 0.5$ there cannot exist any wall.

- *Order parameter m* : The program tries to colorize the spins with 2 colors, so that any 2 neighbouring spins have the same color if and only if there is no wall between them. If a configuration of spins can be uniformly colorized, then the parameter m is defined $m = \frac{|N_1 - N_2|}{N^2}$, where N_1, N_2 are the numbers of spins colorized with the first, and the second color. See Fig.3.2.

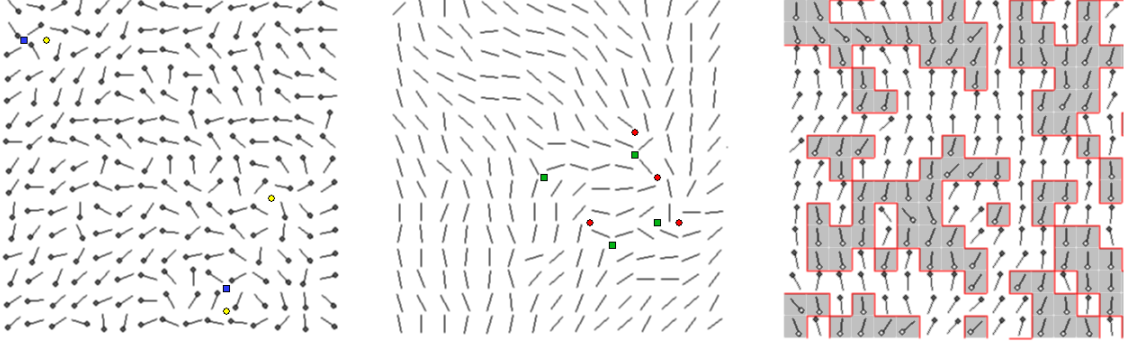


Figure 3.2: Left: Example of vortices identification; vortices are displayed as circles and anti-vortices as squares. In the middle: Example of half-vortices identification; half-vortices are represented by circles and anti-half-vortices by squares. Right: A colorized configuration; the walls are in the picture presented as lines between spins.

3.5 Specific heat

The specific heat (referred to also as heat capacity) of a $N \times N$ square lattice is

$$c = \frac{1}{N^2} \frac{\partial \langle E \rangle}{\partial T}. \quad (3.13)$$

A straightforward way to determine c is to measure precisely $\langle E(T) \rangle$ and $\langle E(T + \Delta T) \rangle$ and to estimate $c(T + \frac{1}{2}\Delta T) \approx \frac{1}{\Delta T} [\langle E(T + \Delta T) \rangle - \langle E(T) \rangle]$. Another possible method is to measure the square of the energy fluctuations, because

$$c = \frac{1}{N^2} \frac{\partial \langle E \rangle}{\partial T} = \frac{1}{N^2} \frac{\partial}{\partial T} \left[\frac{1}{Z(T)} \sum_i E_i e^{-E_i/T} \right] = \frac{\langle E^2 \rangle - \langle E \rangle^2}{N^2 T^2}, \quad (3.14)$$

where $\langle E^2 \rangle - \langle E \rangle^2$ is the square of the standard deviation of energy. The comparison of the evaluated specific heat calculated from differences of energy and from fluctuations of energy is shown in the figure Fig.3.3.

If we want to compare the graphs of specific heat for various j , it is reasonable to normalize the specific heat, so that

$$\int_0^\infty dT C(T) = 1.$$

The normalized specific heat C is then

$$C(T) = \frac{c(T)}{\int_0^\infty dT' c(T')} = \frac{c(T)}{E_{\text{spin}}(T \rightarrow \infty) - E_{\text{spin}}(T \rightarrow 0)} = \frac{c(T)}{0 + 2J(j + j_2)} = \frac{2c(T)}{J(1 + 3j)}. \quad (3.15)$$

3.6 Helicity modulus

The helicity modulus Υ was defined in Sec.2.4, see Eq.(2.50), as

$$\Upsilon = \frac{1}{N^2 a^2} \left. \frac{\partial^2 F}{\partial q^2} \right|_{q=0},$$

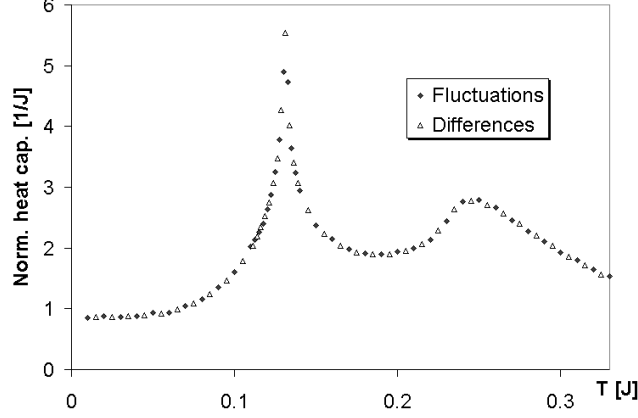


Figure 3.3: The comparison of the evaluated specific heat calculated from differences of energy and from fluctuations of energy. Computed for $j = 0.06$ and the lattice size $N = 128$.

where F is the free energy of the lattice and $q = |\mathbf{q}|$ is the magnitude of gradient \mathbf{q} of externally imposed global twist [6]. The canonical partition function of a lattice without externally imposed global twist is

$$Z_0 = \int \mathcal{D}\theta \exp \left[-\frac{\sum_{\langle kl \rangle} e(\Delta\theta_{kl})}{T} \right], \quad (3.16)$$

where $\Delta\theta_{kl}$ is a short denotation for $\theta_k - \theta_l$. The canonical partition function for $\mathbf{q} \neq \mathbf{0}$ expanded to the 2nd order of q is

$$\begin{aligned} Z(q) &= \int \mathcal{D}\theta \exp \left[-\frac{\sum_{\langle kl \rangle} e(\Delta\theta_{kl} + \mathbf{q} \cdot \mathbf{r}_{kl})}{T} \right], \\ &= \int \mathcal{D}\theta \exp \left[-\frac{\sum_{\langle kl \rangle} \left[e(\Delta\theta_{kl}) + e'(\Delta\theta_{kl}) \mathbf{q} \cdot \mathbf{r}_{kl} + \frac{1}{2} e''(\Delta\theta_{kl}) (\mathbf{q} \cdot \mathbf{r}_{kl})^2 \right]}{T} \right], \\ &= Z_0 \left\langle \exp \frac{-1}{T} \left[\sum_{\langle kl \rangle} e'(\Delta\theta_{kl}) \mathbf{q} \cdot \mathbf{r}_{kl} + \frac{1}{2} \sum_{\langle kl \rangle} e''(\Delta\theta_{kl}) (\mathbf{q} \cdot \mathbf{r}_{kl})^2 \right] \right\rangle_0, \\ &= Z_0 \left[1 - \frac{1}{T} \sum_{\langle kl \rangle} \langle e'(\Delta\theta_{kl}) \rangle_0 \mathbf{q} \cdot \mathbf{r}_{kl} - \frac{1}{2T} \sum_{\langle kl \rangle} \langle e''(\Delta\theta_{kl}) \rangle_0 (\mathbf{q} \cdot \mathbf{r}_{kl})^2 + \frac{1}{2T^2} \left\langle \left(\sum_{\langle kl \rangle} e'(\Delta\theta_{kl}) \mathbf{q} \cdot \mathbf{r}_{kl} \right)^2 \right\rangle_0 \right], \end{aligned}$$

where $\mathbf{r}_{kl} \equiv \mathbf{r}_k - \mathbf{r}_l$ is the vector connecting the nearest neighbours. Now, we can use the symmetry of the bond energy $e(\Delta) = e(-\Delta) \Rightarrow e'(\Delta) = -e'(-\Delta)$, therefore $\langle e'(\Delta\theta_{kl}) \rangle_0 = 0$. Free energy to the 2nd order in q is then

$$F(q) = -T \ln Z(q) = F_0 + \frac{q^2}{2} \sum_{\langle kl \rangle} \langle e''(\Delta\theta_{kl}) \rangle_0 (\mathbf{n} \cdot \mathbf{r}_{kl})^2 - \frac{q^2}{2T} \left\langle \left(\sum_{\langle kl \rangle} e'(\Delta\theta_{kl}) \mathbf{n} \cdot \mathbf{r}_{kl} \right)^2 \right\rangle_0, \quad (3.17)$$

where \mathbf{n} is the unit vector in the direction \mathbf{q} defined by $\mathbf{q} = q\mathbf{n}$. If we choose $\mathbf{n} = \frac{1}{\sqrt{2}}(1, 1)$ then the helicity modulus equals

$$\Upsilon = \frac{1}{2N^2} \langle E^{(2)} \rangle - \frac{1}{2N^2 T} \langle [E^{(1)}]^2 \rangle, \quad (3.18)$$

where $E^{(1)}$ and $E^{(2)}$ are defined in Sec.3.4.

3.7 Susceptibilities

If M is an extensive quantity and B is field conjugate to M , then the field M contributes to the energy with the term $-MB$. The partition sum is therefore

$$Z(B) = \sum_n e^{-\frac{E_n - M_n B}{T}} \quad (3.19)$$

and the average M is

$$\langle M(B) \rangle = \frac{1}{Z(B)} \sum_n M_n e^{-\frac{E_n - M_n B}{T}}. \quad (3.20)$$

The susceptibility is

$$\chi \equiv \frac{1}{N^2} \left. \frac{\partial \langle M \rangle}{\partial B} \right|_{B=0} = \frac{1}{N^2 T} \left[\langle M^2 \rangle_{B=0} - \langle M \rangle_{B=0}^2 \right], \quad (3.21)$$

where $\langle X \rangle_{B=0}$ stands for the average value of the quantity X for $B = 0$. The susceptibility corresponding to magnetization M_x is then $\chi_{1,x}$, and for M_y it is $\chi_{1,y}$. We calculate the magnetic susceptibility as¹³

$$\chi_1 = \frac{\chi_{1,x} + \chi_{1,y}}{2} = \frac{1}{2N^2 T} \left[\langle M_x^2 \rangle + \langle M_y^2 \rangle - \langle M_x \rangle^2 - \langle M_y \rangle^2 \right]. \quad (3.22)$$

The nematic susceptibility is then similarly

$$\chi_2 = \frac{1}{2N^2 T} \left[\langle N_x^2 \rangle + \langle N_y^2 \rangle - \langle N_x \rangle^2 - \langle N_y \rangle^2 \right]. \quad (3.23)$$

In the magnetic phase, both – the magnetic and the nematic – susceptibilities diverges with $N \rightarrow \infty$. In the paramagnetic phase are both susceptibilities extremely local, and thus insensitive to the finite-size scaling.¹⁴ In the nematic phase is due to the loss of spin-orientation order the magnetic susceptibility local and thus independent on N . Surely, the nematic susceptibility diverges with $N \rightarrow \infty$ in the nematic phase.

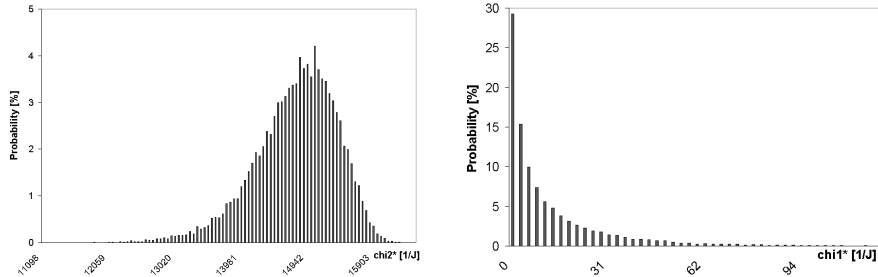


Figure 3.4: Left: Typical histogram of susceptibility in the ordered phase concerning the specific susceptibility; namely it is histogram for χ_2^* computed for $N = 64$, and $j = 0.02$, at $T = 0.1 J$. Right: Typical histogram of susceptibility in the disordered phase concerning the specific susceptibility; it is the histogram for χ_1^* computed for $N = 64$, and $j = 0.02$, at $T = 0.1 J$.

3.8 Identification of the KT phase transition

According to [12], the theoretical helicity modulus $\Upsilon_N^*(T)$ of a lattice $N \times N$ at temperature $T \rightarrow T_2^-$ in the limit for large N is

$$\Upsilon_N^*(T) = \Upsilon_\infty(T) \left[1 + \frac{1}{2} \frac{1}{\ln N + C} \right], \quad (3.24)$$

¹³The terms $\langle M_x \rangle^2$, and $\langle M_y \rangle^2$, may be neglected in the formula for the magnetic susceptibility, because the problem has rotational symmetry – i.e. if we rotate each spin by a fixed angle α , then the energy (and thus also the probability of occurrence) will not change. I have checked that the terms $\langle M_x \rangle^2$, and $\langle M_y \rangle^2$ are always of smaller order than the terms $\langle M_x^2 \rangle$, and $\langle M_y^2 \rangle$. The magnetic susceptibility with neglected terms $\langle M_x \rangle^2$, and $\langle M_y \rangle^2$ is then $\chi_1^* = \frac{1}{2N^2 T} \langle |\mathbf{M}|^2 \rangle$.

¹⁴The reason is following: the lattice $N \times N$ spins has $n \equiv N^2$ spins. Thus, in the disordered paramagnetic phase the magnitude of the total magnetization $|\mathbf{M}|$ is proportional to \sqrt{n} , where we have made use of random walk. Since the susceptibility is $\chi_1^* = \frac{1}{2nT} \langle |\mathbf{M}|^2 \rangle$, it is clear that in the paramagnetic phase are both susceptibilities independent on n .

where C is a constant, T_2 is the critical temperature of the KT phase transition and $\Upsilon_\infty(T)$ is the universal jump of the helicity modulus in an infinite lattice. For the KT phase transition due to vortex unbinding is the jump equal to $\frac{2T}{\pi}$, and for the KT phase transition due to half-vortex unbinding it is $\frac{8T}{\pi}$. The formula Eq.(3.24) follows the KT equations Eq.(2.27) (for half-vortex unbinding Eq.(2.37)) analysed near the fixed point, using the asymptotic solution Eq.(2.30) (for half-vortices: Eq.(2.39)).¹⁵ One possible way to determine the transition temperature T_2 is

1. to numerically compute $\Upsilon_N(T)$ for M different (large) N
2. fit the constant C and find the minimum of

$$\delta^2 = \frac{1}{M} \sum_{i=1}^M [\Upsilon_{N_i}^*(T) - \Upsilon_{N_i}(T)]^2, \quad (3.25)$$

where δ will be referred to as the root-mean-square error of the fit; the values $\Upsilon_N(T)$ are results of numerical experiments. With the scaling formula it is also possible to verify the value of the universal jump when we do a fit with 2 fitting parameters: the constant C and the universal jump Υ_∞ .

Another method is to use the finite-size scaling of the susceptibilities. Spin-wave low-temperature theory¹⁶ predicts that the magnetic susceptibility χ_1 is proportional to $N^{2-\frac{T}{2\pi J}}$, and nematic susceptibility χ_2 is proportional to $N^{2-\frac{2T}{\pi J}}$ [11]. At the transition temperature the coupling constant J is due to renormalization (see Sec.2.4) effectively equal to the jump of the helicity modulus Υ . Thus we obtain for the transition temperature the finite-size scalings $\chi_1 \propto N^{7/4}$, and $\chi_2 \propto N^{4/4}$ for the KT phase transition due to vortex unbinding. For the KT phase transition due to half-vortices we obtain $\chi_2 \propto N^{7/4}$.¹⁷ According to [13], the drawback of these susceptibility scalings is that the ansatz is too simple – the helicity modulus Υ in a finite lattice is larger than the universal jump at T_2 (see the 1st order prediction is Eq.(3.24)) – therefore this method is less accurate.

¹⁵We may consider that by computing Υ on a lattice $N \times N$ we compute $K[\ln(cN)]$. Then the constant C is $\ln c$.

¹⁶The spin-wave low-temperature theory is calculated using the low-temperature harmonic Hamiltonian Eq.(1.4).

¹⁷For the magnetic susceptibility we obtain $\chi_1 \propto N^{31/16}$, but the finite-size scaling for the magnetic susceptibility is unusable since the nematic phase is concerning the J_1 -interaction already a high-temperature (disordered) phase.

Chapter 4

Results of numerical experiments

The numerical results were obtained on square lattices $N \times N$ with periodic boundary conditions, mostly using Wolff's algorithm and for linear dimensions $N = 32, 64, 128, 256$ and 512 . The results were compared with the results obtained by the Metropolis algorithm on smaller lattices $N = 32, 64$. Typically, a numerical experiment follows these steps:

1. Creating an initial configuration. This can either be a random configuration, when cooling down from high temperatures; or a frozen configuration, $\forall i : \theta_i = 0$ when heating up from low temperatures.
2. Thermalization for a selected temperature. This includes Monte Carlo (MC) steps without measurements counting into the averages. The number of necessary MC steps depends mostly on the lattice size and the temperature step.¹ We used overestimation of necessary MC steps for energy thermalization. Typically, for convenient temperature steps $\sim 0.05J$ and Wolff's algorithm we used the following numbers of MC steps: ~ 50000 for $N \leq 128$; ~ 100000 for $N = 256$; ~ 250000 for $N = 512$.
3. Measurements: in this step the program executes one measurement of the observed quantities after k MC steps. We can regulate the (in)dependency of measured quantities with the number k – higher k provides for lower values of autocorrelation function $R_x(\tau)$ (see section Sec.3.3) for measured quantity x and therefore increases the number of *effectively independent measurements* of x .
4. Temperature change and back to step 2.

The number of measurements was usually $20000 - 40000$ and on smaller lattices up to 100000 to provide small error bars of intensive quantities; on the largest lattice 512×512 , the number of measurements was sometimes only 10000 . The results obtained by heating the lattice from low temperatures (initial phase was totally ordered) compared with the results obtained by cooling down from high temperatures (initial phase disordered) are identical within the error bars when the temperature changes are at least one order smaller than typical temperature difference on the temperature scale (e.g. the temperature region of a particular phase) and the time for thermalization is sufficient.

4.1 Numerical results for $j = 1$

For the XY model we know that at $T_2 = 0.89294(8)$ [14] there occurs a phase transition of the KT type. The energy (and heat capacity) should be a C^∞ function. The graphs of energies per spin for $N = 32, 64, 128, 256$ are almost identical. A small difference is observable in the graph of the heat capacity, where the peak moves with increasing N leftwards and drops slightly. At temperatures above T_2 the vorticity grows rapidly. The graphs of vorticity as a function of temperature are identical for various lattice sizes N , therefore I plot the vorticity only for $N = 64$. The graph of the helicity modulus $\Upsilon_N(T)$ for various N reveals evidently the tendency that $\Upsilon_N(T)$ is at the predicted transition temperature T_2 steeper for larger N – see Fig.4.1.

From the graph of the helicity modulus as a function of T it is possible to determine the temperature point closest to T_2 using the finite-size scaling (see Sec.3.8); in our case the lowest root-mean-square error δ is

¹Since a Wolff's MC step has impact on many spins, the number of necessary MC steps for the Metropolis algorithm is larger of the order of the Wolff's cluster area size.

realized for $T_2 = 0.89 J$; see Fig.4.2. Another method to determine T_2 is to find the intersection of $\chi_1/N^{7/4}$, or the intersection of $\chi_2/N^{4/4}$, for various N . Both intersections lie little above the known estimate of T_C , at $T \approx 0.905 J$ and at $T \approx 0.91 J$, respectively; see Fig.4.3. Results of all three scalings are consistent with known results and thus we have a successful test of the methods and numerical computation itself.

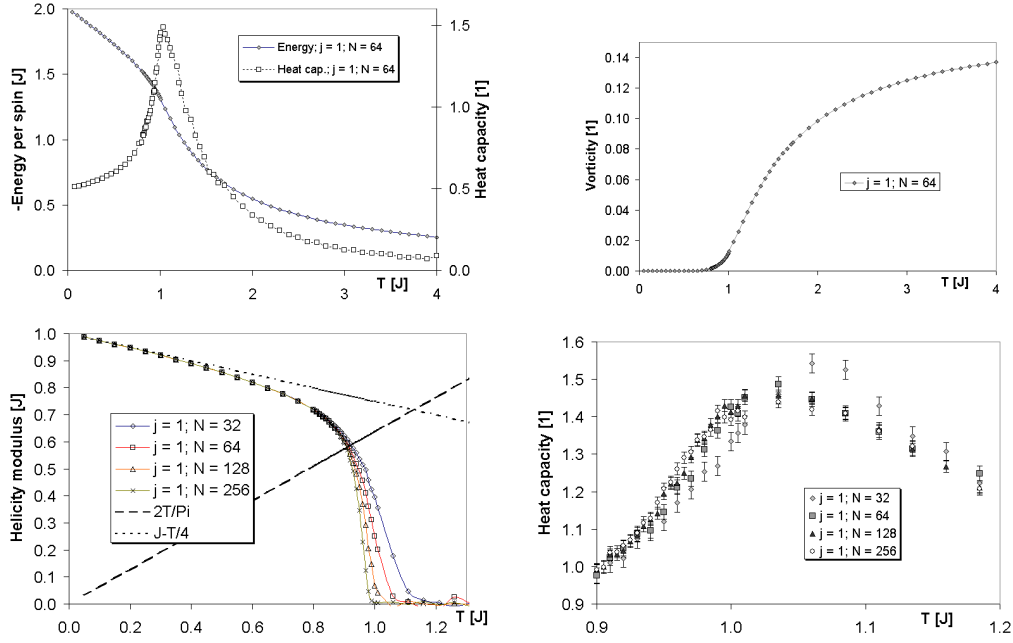


Figure 4.1: Graphs of the energy $E(T)$, heat capacity $c(T)$, and vorticity $V(T)$ for $j = 1$ and $N = 64$. Below there is the plot of the helicity modulus $\Upsilon_N(T)$ and a detail of the specific heat peak for $j = 1$ and $N = 32, 64, 128, 256$. In the graph of the helicity modulus, there is also the line $\frac{2T}{\pi}$ showing the universal jump, and the line $J - \frac{T}{4}$ displaying the renormalization of J due to anharmonicity. The lines between the measured points are only guides for eyes – as it is each time in this paper. The error bars are smaller than the symbols showing the measured values – as it is each time in this paper unless the error bars are displayed.

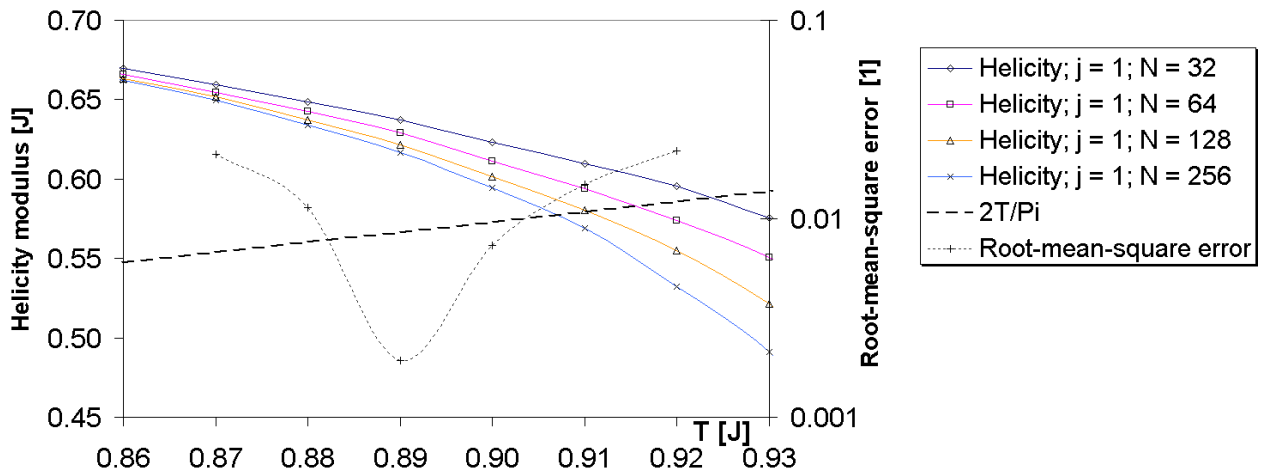


Figure 4.2: Detail of the graph of the helicity modulus $\Upsilon_N(T)$ for $j = 1$ and lattice sizes $N = 32, 64, 128, 256$. The plot also includes the prediction of the universal jump $\frac{2T}{\pi}$ and the root-mean-square error δ of the 1-parametrical fit (with fixed jump $\frac{2T}{\pi}$) of the helicity modulus (see Sec.3.8).

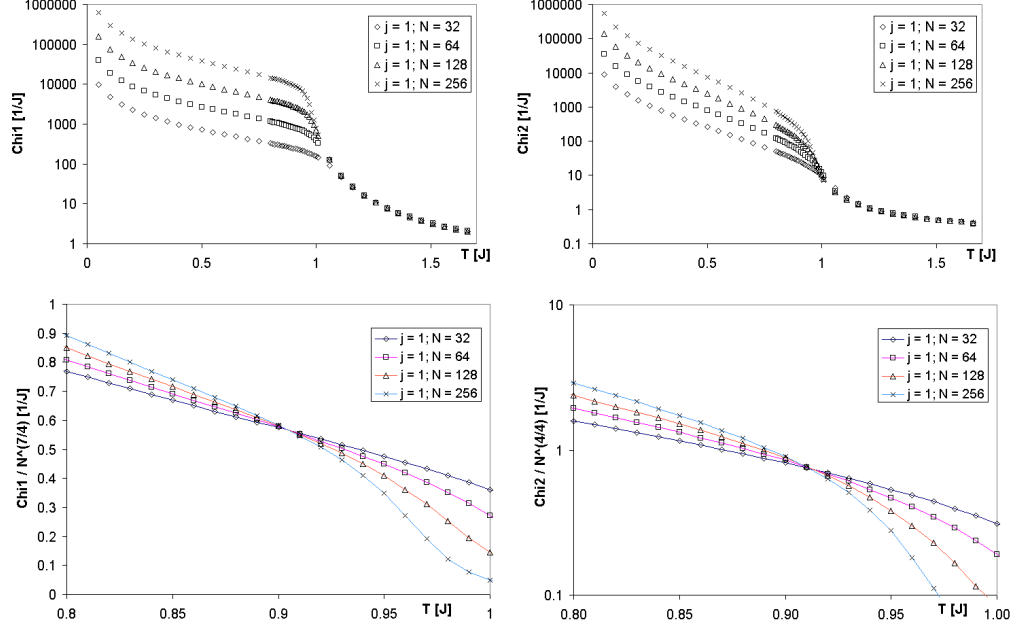


Figure 4.3: Graphs of the magnetic and nematic susceptibilities $\chi_1(T)$ and $\chi_2(T)$ for $j = 1$ and $N = 32, 64, 128, 256$ in logarithmic scale vs. temperature. The lower pictures show the finite-size scaling of $\chi_1(T)$ and $\chi_2(T)$ to estimate the phase-transition temperature for $j = 1$.

4.2 Numerical results for $j = 0$

If we take into account the equation describing the averages of analogous functions Eq.(1.14), we obtain following relations

- for energy $\langle E^{[0]}(T) \rangle = \frac{1}{4} \langle E^{[1]}(4T) \rangle$, thus the specific heat is $c^{[0]}(T) = \frac{\partial \langle E^{[0]} \rangle}{\partial T} = c^{[1]}(4T)$,
- for helicity modulus $\Upsilon^{[0]}(T) = \Upsilon^{[1]}(4T)$,
- for susceptibility $\chi_2^{[0]}(T) = 4\chi_1^{[1]}(4T)$,
- for half-vorticity: mean half-vorticity V_H for $j = 0$ at temperature T is the same as mean vorticity V for $j = 1$ at $4T$.

Numerical results for energy $E(T)$, specific heat capacity $c(T)$, half-vorticity as a function of T , helicity modulus $\Upsilon(T)$ and nematic susceptibility $\chi_2(T)$ are, according to the previous paragraph, identical within the error bars with the results for $j = 0$.

The vortex identification is totally irrelevant, because the orientation of spins is random and an arbitrarily small direction variance of the spins might cause a positive identification of a vortex at all temperatures. The vorticity is almost constantly 17%. The magnetic susceptibility is the same for all inspected lattice sizes ($N = 32, 64, 128, 256$), approximately $\chi_1 \approx \frac{1}{2T}$; see Fig.4.4.

The KT phase transition temperature is $T_2(j = 0) = T_2(j = 1)/4 = 0.223 J$.

4.3 Numerical results for $j = 0.02$

The case $j = 0.02$ is our representant of sufficiently small j from the estimate in Sec.1.2.3. According to our hypothesis, there should exist 3 phases and 2 phase transitions. We may consider the model with $j = 0.02$ as a small modification of the case $j = 0$; for better comparison we will use units J_2 independent on j . The graph of energy per spin for $j = 0.02$ compared with the graph of energy per spin for $j = 0$ suggests a phase

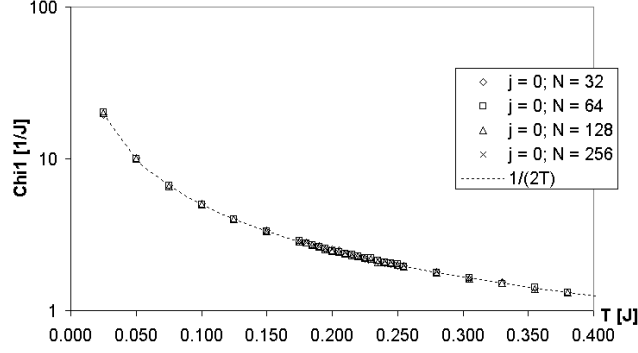


Figure 4.4: For $j = 0$, the magnetic susceptibilities $\chi_{1,N}(T)$ are the same for $N = 32, 64, 128, 256$; $\chi_1 \approx \frac{1}{2T}$.

transition at $T \approx 0.05 J$.² The graph of the magnetic susceptibility shows that below $T \approx 0.05 J$ there exists a magnetic phase. The graphs of the nematic susceptibility and the half-vorticity show that above $T \approx 0.05 J$ there exists a nematic phase (as for $j = 0$) up to $T_2 \approx 0.22 J$. The comparison of graphs of the helicity modulus, the energy and the nematic susceptibility for $j = 0.02$ and for $j = 0$ clearly reveal that the phase transition at T_2 remained without changes.

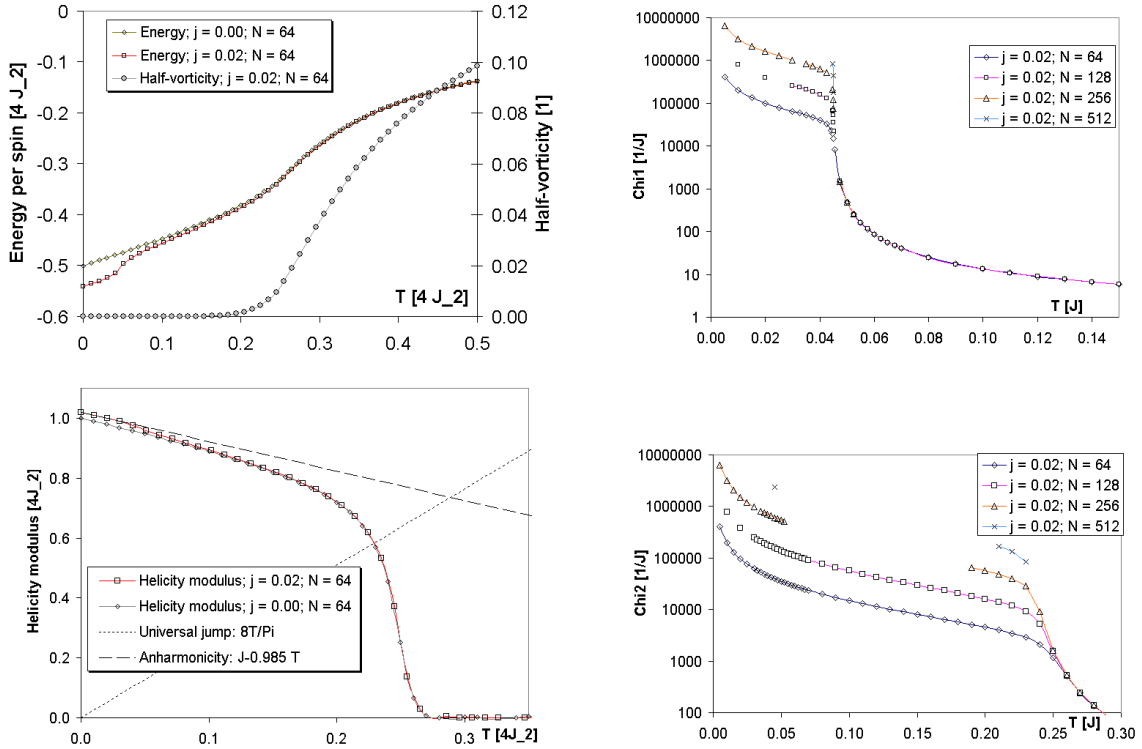


Figure 4.5: Comparison of energies per spin between $j = 0.02$ and $j = 0$ in units $4J_2$ for lattice $N = 64$. Graph of half-vorticity for $j = 0.02$, $N = 64$ as a function of temperature. The comparison of helicity modulus between $j = 0.02$ and $j = 0$ for $N = 64$ with displayed renormalization due to anharmonicity for $j = 0.02$ and with the universal jump $\frac{8T}{\pi}$. Graphs of the magnetic susceptibility $\chi_{1,N}(T)$ and the nematic susceptibility $\chi_{2,N}(T)$ for $j = 0.02$ and $N = 64, 128, 256, 512$.

Representative configurations³ near the critical temperature $T_1 \approx 0.045 J$ show a pattern known from the

²The graph of energy per spin comparing the cases $j = 0$ and $j = 0.02$ is drawn in natural units $4J_2$. The unit J is for $j < 1$ equivalent to $J = \frac{4J_2}{1-j}$.

³The configurations were selected in that way that their parameter m is approximately equal to the average $\langle m \rangle$ for the

Ising model [15] – see Fig.4.6.

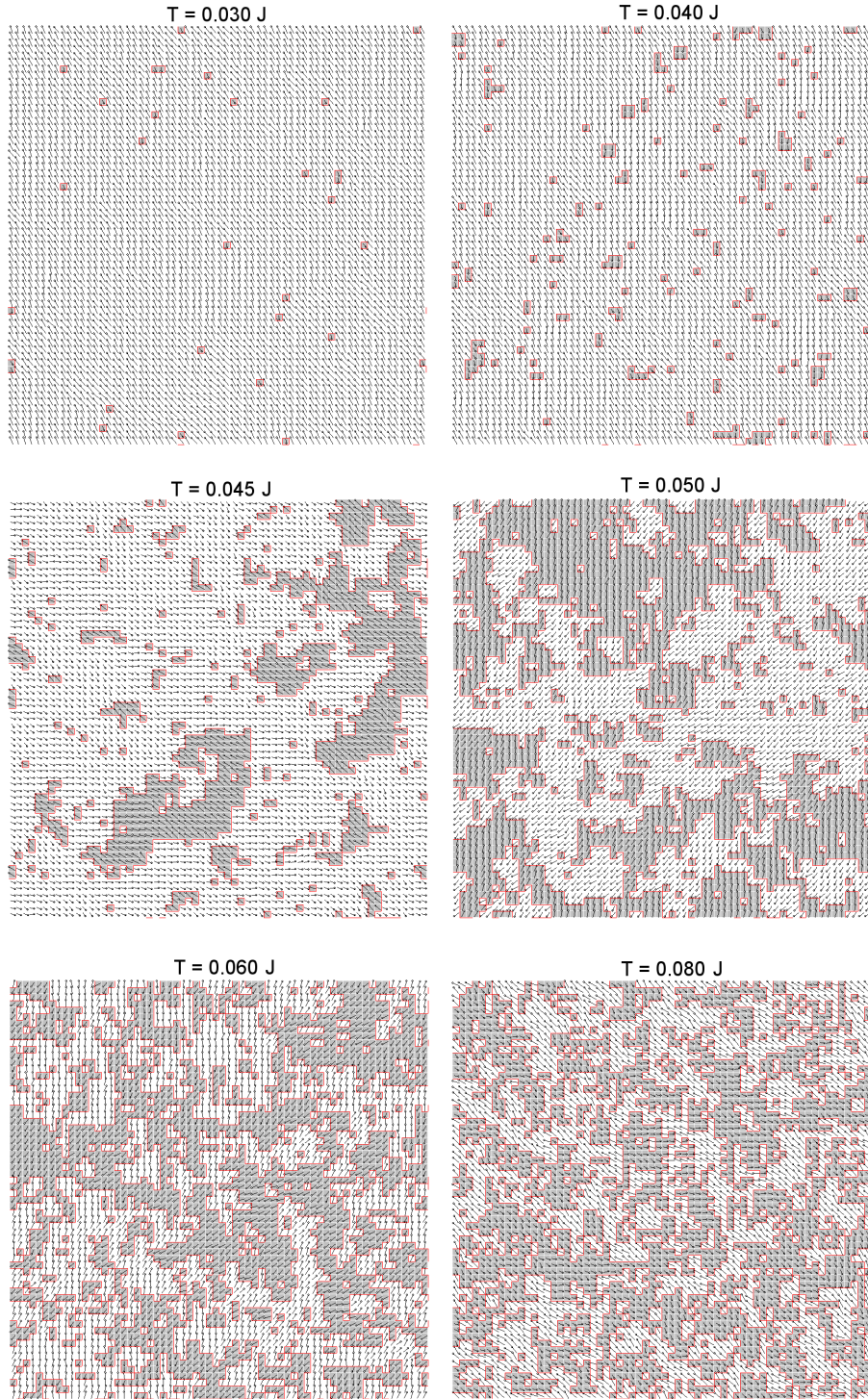


Figure 4.6: Representative configurations for $j = 0.02$ and $N = 64$ when passing the Ising phase transition.

The upper phase transition at $T_2 \approx 0.22 J$ was investigated using the finite-size scaling of the helicity modulus, and of the nematic susceptibility. The temperatures $T_2(j = 0.02)$ of the phase transition determined from the helicity and the nematic susceptibility are consistent, $T_2 \approx 0.22 J$; see Fig.4.7. According to [12], the particular temperature.

finite-size scaling formula Eq.(3.24) of the helicity modulus is in fact valid to extremely good approximation down to small lattice sizes, in the model with $j = 1$ (and thus according to the similarity Sec.1.2.1 also for $j = 0$). Therefore we have computed the helicity modulus (with high accuracy $\pm 0.0001 J$; the number of measurements was 5000000) for lattice sizes $n = 16, 20, 24, 28, 32, 36, 40, 48$ and done 2-parametrical fit of the data for each inspected temperature point, see Fig.4.8. The universal jump in the helicity modulus is $\frac{8T}{\pi}$ with tolerance $\pm 6\%$.

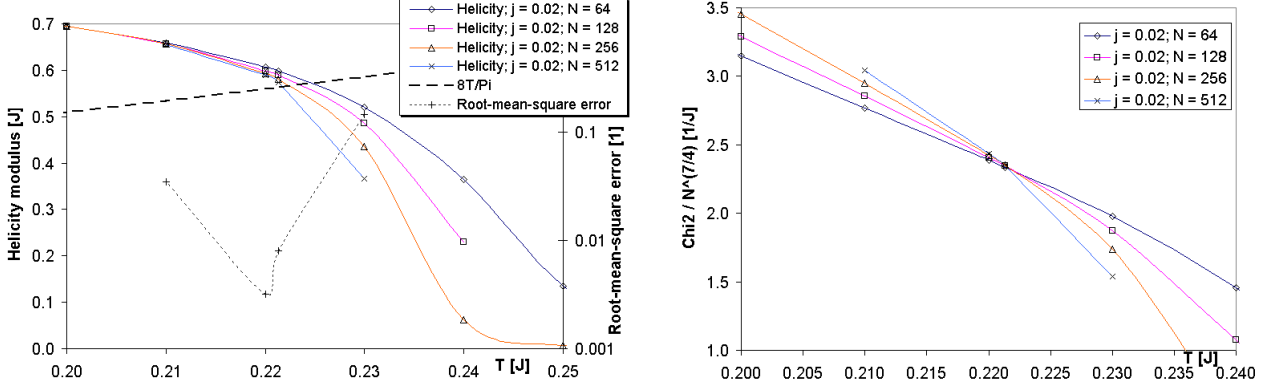


Figure 4.7: Left: Graph of the helicity modulus for $j = 0.02$ and $N = 32, 64, 128, 256$ vs. temperature in detail. The figure includes the mean-square error δ of the 1-parametrical fit of the helicity modulus and the universal jump $\frac{8T}{\pi}$. Right: Graph of the scaled nematic susceptibility $\chi_2 / N^{7/4}$ to estimate the phase-transition temperature $T_2(j = 0.02)$.

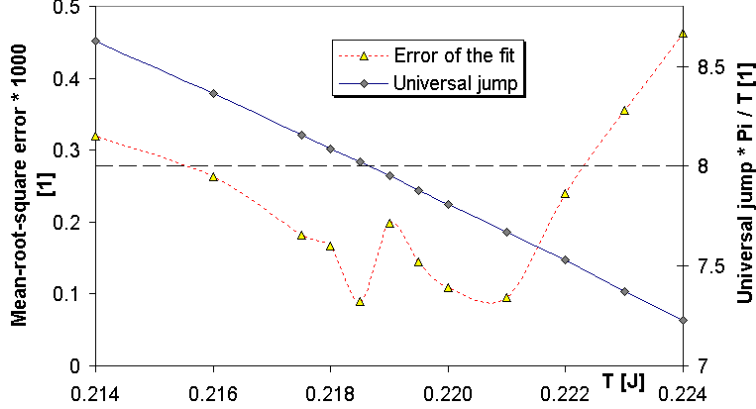


Figure 4.8: Graph of the universal jump and mean-root-square error of the 2-parametrical fit of the helicity modulus Υ_N as a function of temperature, fitted for $N = 16, 20, 24, 28, 32, 36, 40, 48$; $j = 0.02$.

The autocorrelation times exploded at the lower critical temperature T_1 . The temperature with the largest autocorrelation time drifts slightly to low temperatures, like the peak of the heat capacity. For the largest investigated lattice with $N = 512$ the critical temperature was $T_1 = 0.0449 J$.

The heat capacity at the potentially Ising-like transition at $T \approx 0.045 J$ grows for larger lattices. The peak is localised at the same temperature as the steepest increment of the walls; see Fig.4.9. The heat capacity of the Ising model at the critical temperature should be approximately $A + B \ln N$, where A and B are constants [16]. Therefore we also plotted the graph of the differential heat capacity $c_{\text{diff}}(T) \equiv c_{0.02}(T) - c_0(T)$, where $c_x(T)$ is the heat capacity for $j = x$. The increments of the peaks for doubled N should be the same if the transition would be Ising-like. The values do satisfy this criterion within the error bars. The critical temperature T_1 is estimated from the maximum of the heat capacity peak for the largest lattice with linear size $N = 512$, $T_1 = 0.0449 J$; see Fig.4.10.

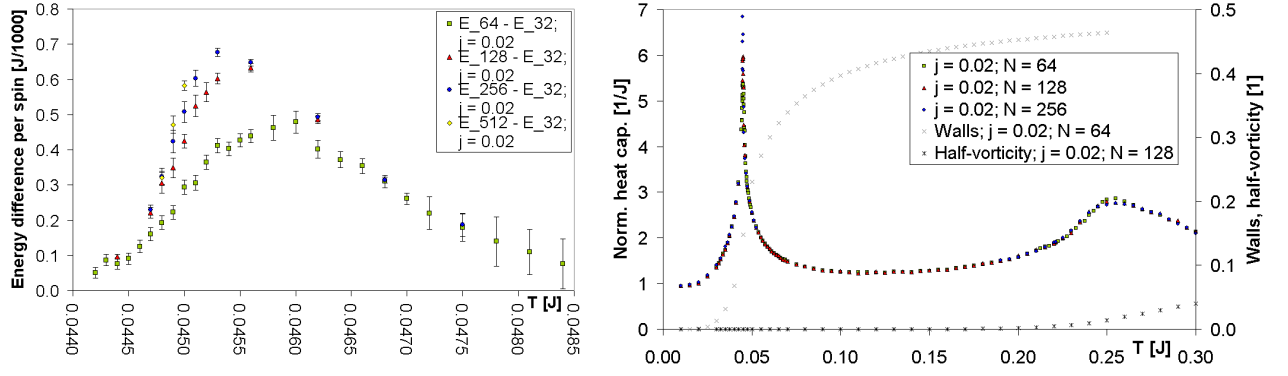


Figure 4.9: Left: The graph showing the difference of energy per spin $E_N(T) - E_{32}(T)$ close to $T = 0.045 J$ for $j = 0.02$ and $N = 64, 128, 256, 512$. Right: the normalized specific heat for $j = 0.02$ and $N = 64, 128, 256$ together with the number of walls per spin for (for $N = 64$) and half-vorticity (for $N = 128$) as functions of temperature, both for $j = 0.02$.

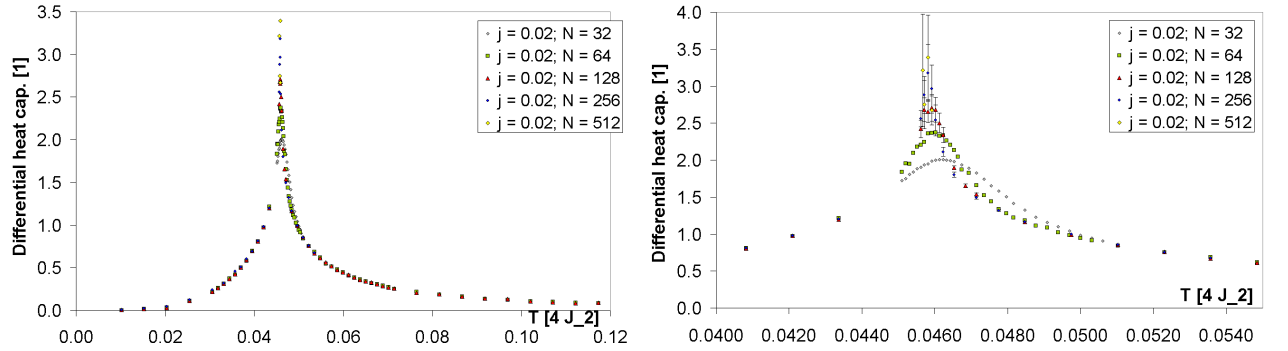


Figure 4.10: The differential heat capacity $c_{0.02}(T) - c_0(T)$ for various lattice sizes N on a large scale and in detail with error bars. The heat capacity $c_{0.02}(T)$ is computed from fluctuations, the heat capacity $c_0(T)$ is computed from energy differences. The temperature scale is in units $4J_2 = 0.98 J_{0.02}$.

I have also calculated the increase of entropy corresponding to the differential heat capacity

$$S_{\text{diff}} = \int_0^{T_{\text{max}}} \frac{c_{\text{diff}}(T)}{T} dT = \int_0^{T_{\text{max}}} \frac{dE_{\text{diff}}}{T} \approx \sum_i \frac{E_{\text{diff}}(T_{i+1}) - E_{\text{diff}}(T_i)}{(T_{i+1} + T_i)/2}, \quad (4.1)$$

where T_i are examined temperature points. For the lattice with linear size $N = 128$ with an upper cut off at $T_{\text{max}} = 0.30 J$ and about 60 (non-uniformly distributed) temperature points I obtained the increase of entropy per spin $S_{\text{diff}} \approx 0.714$. The calculation for $N = 64$ with higher density of investigated temperature points (about 120, again non-uniformly distributed) up to $T = 0.50 J$ gives $S_{\text{diff}} \approx 0.702$ per spin. Both of these values are close to the increase of entropy in the Ising model, $\Delta S_{\text{Ising}} = \ln 2 \approx 0.693$ and contribute to verifying the expectation that the transition magnetic-nematic is of the Ising type.

If the parameter m (see Sec.3.4) is an order parameter (for $N \rightarrow \infty$) and the phase transition at $T_1 \approx 0.045 J$ is really of the Ising type, then the order parameter in the neighbourhood of T_1 should be proportional to $(T_1 - T)^{1/8}$ for $T < T_1$ and $m \equiv 0$ for $T > T_1$.⁴ The values were fitted for $T_1 = 0.0449$ estimated from the heat capacity peak; see Fig.4.11.

⁴The last condition is for $N \rightarrow \infty$ satisfied because of the law of large numbers. According to the law of large numbers, for temperatures $T > T_1$, $m_{2N}(T) = \frac{1}{2}m_N(T)$ should hold, which seems to be true.

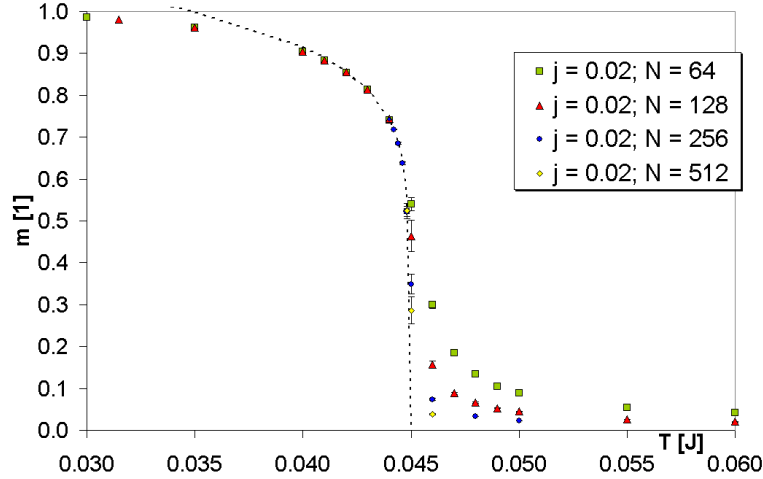


Figure 4.11: Graph of parameter $m(T)$ for $j = 0.02$ and $N = 64, 128, 256, 512$, including fit for the (possibly order) parameter m with an Ising exponent, $m \propto (T_1 - T)^\delta$ with $\delta = 1/8$ and $T_1 = 0.0449 J$.

4.4 Numerical results for $j = 0.16$

The model with $j = 0.16$ should represent the case without the nematic phase. The graph of energy $E(T)$ reveals only one region with higher heat capacity. The peak in heat capacity moves slightly towards lower temperatures with increasing lattice size N , but does not grow.

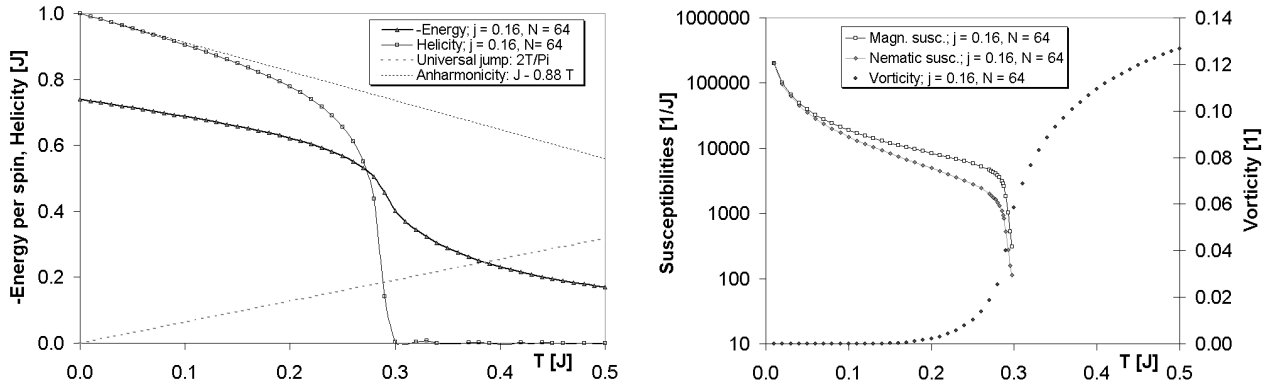


Figure 4.12: Left: Graph of the energy $E(T)$ and the helicity modulus $\Upsilon(T)$ for $j = 0.16$ and $N = 64$. The dotted lines are the universal jump $\frac{2T}{\pi}$ for the helicity and the prediction of Υ from J renormalization due to anharmonicity (see Eq.(2.51)). Right: Vorticity $V(T)$ and plots of the magnetic and nematic susceptibility, $\chi_1(T)$ and $\chi_2(T)$, all for $j = 0.16$ and $N = 64$.

The phase transition was dealt with the same techniques as the KT phase transition for $j = 1$, using the fit for helicity with the universal jump $\frac{2T}{\pi}$ and inspecting the intersections of $\chi_1/N^{7/4}$, and $\chi_2/N^{4/4}$. The estimated phase-transition temperature is consistently $T_2 \approx 0.287 J$; see Fig.4.13. The 2-parametrical fit of the helicity modulus performed with values $\Upsilon_N(T)$ for $N = 64, 128, 256, 512$ at temperature points $T = 0.2850, 0.2865, 0.2875 J$ determines the universal jump between $\frac{1.45T}{\pi}$ and $\frac{2.9T}{\pi}$.

4.5 The phase diagram

Our final effort was to construct the phase diagram in the space (plane) of parameters j and T ; see Fig.4.16. The transitions for $j = 0, 0.02, 0.16, 1$ were studied intensively. For $j = 0.04, 0.06, 0.10, 0.14$ the transition temperatures $T_2(j)$ were found by finite-size scaling of susceptibilities using only 2 lattice sizes $N = 64, 128$.

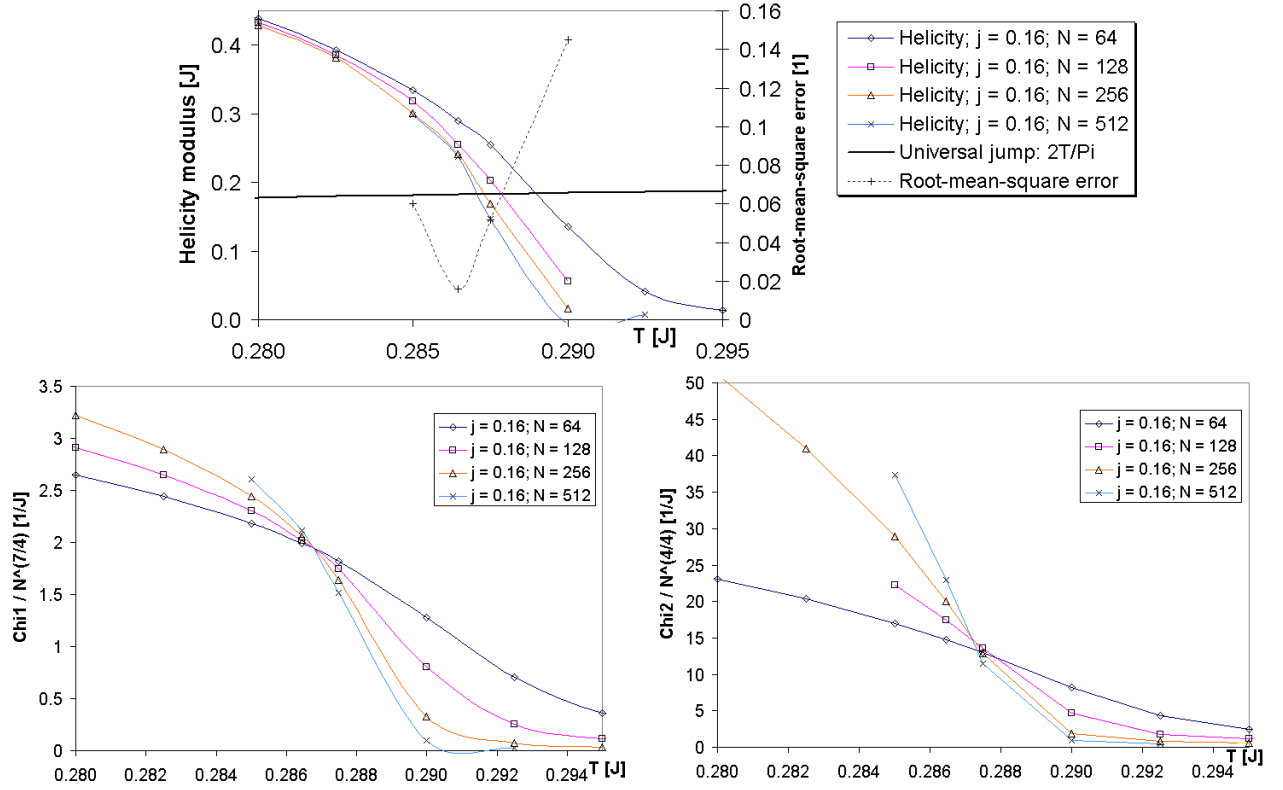


Figure 4.13: Detailed graph of the helicity modulus with the root-mean-square-error δ of the 1-parametrical finite-size-scaling fit, for $j = 0.16$. Lower graphs: determination of the transition temperature $T_2(j = 0.16)$ from the finite-size scalings $\chi_1/N^{7/4}$, $\chi_2/N^{4/4}$ of the susceptibilities.

For $j = 0.2, 0.3, \dots, 0.9$ the transition temperatures $T_2(j)$ were found roughly from the graphs of the magnetic susceptibilities $\chi_1(T)$; the transition temperature $T_2(j)$ in units J rises approximately linearly with j from $T_2(j = 0.16) \approx 0.29 J$ up to $T_2(j = 1) \approx 0.89 J$.

The lower transition temperature $T_1(j)$ was determined from the peak of the specific heat. The estimate of the magnetic-nematic phase transition temperature $T_1(j)$ outgoing from the conception of an Ising-like phase transition seems to be very close to the obtained results and thus it is a next argument supporting the conception.

Although the triple point was not inspected seriously, we have inspected the models with $j = 0.08, 0.12$ with special care. The neighbourhood of the transitions was inspected using the finite-size scalings of both susceptibilities.⁵ The observables were computed on lattices with linear sizes $N = 32, 64, 128, 256, 512$. The jump of the helicity was observed, too.

- The model with $j = 0.08$ has still well separated phase transitions. The magnetic susceptibility is already attenuated at $T_2(j = 0.08) \approx 0.215$, the finite-size scaling of the nematic susceptibility $\chi_2 N^{7/4}$ intersect with high precision at $T_2(j = 0.08) \approx 0.2165 J$. See Fig.4.14. The 2-parametric fit of the helicity modulus for the temperatures $T = 0.2075, 0.2100, 0.2125, 0.2150, 0.2175 J$ with $N = 64, 128, 256, 512$ gives jumps in the range from $\frac{8.35T}{\pi}$ to $\frac{9.3T}{\pi}$ with unestimated accuracy.⁶
- The model with $j = 0.12$ is rather complicated – the vicinity of the triple point results also in increasing autocorrelation times.⁷ The data is unclear: the finite-size scaling $\chi_2/N^{4/4}$ does not intersect well,

⁵The nematic susceptibility was used in both possible finite-size scalings $\chi_2 N^{7/4}$ and $\chi_2 N^{4/4}$.

⁶The root-mean-square error δ of the 2-parametric fit of the helicity has not a well localized minimum. Therefore this method (fitting values of $\Upsilon_N(T)$ for only 4 lattice sizes, and with relatively high error bars $\sim 0.002 J$) is inappropriate for determination of the transition temperature.

⁷For a finite lattice is our argument (from beginning of Sec.2.1) that at the magnetic-paramagnetic phase transition do half-vortices not play a role, not valid. Therefore complicated finite-size effects may arise in the vicinity of the triple point .

but both, the finite-size scaling $\chi_1/N^{7/4}$, and $\chi_2/N^{7/4}$ intersect well. The magnetic susceptibility seems to diverge with $N \rightarrow \infty$. The 2-parametrical fit of the helicity for the temperatures $T = 0.2350, 2375, 2400, 2425 J$ with $N = 64, 128, 256, 512$ estimates the universal jump in the range from $\frac{6.15T}{\pi}$ to $\frac{7.8T}{\pi}$. See Fig.4.15.

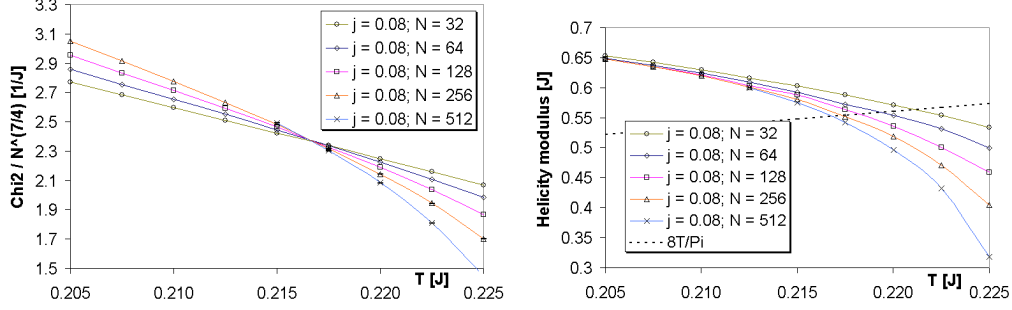


Figure 4.14: Left: The finite-size scaling of the nematic susceptibility $\chi_2 N^{7/4}$ for determination of $T_2(j = 0.08)$. Right: The helicity modulus $\Upsilon_N(T)$ for $j = 0.08$ and $N = 32, 64, 128, 256, 512$.

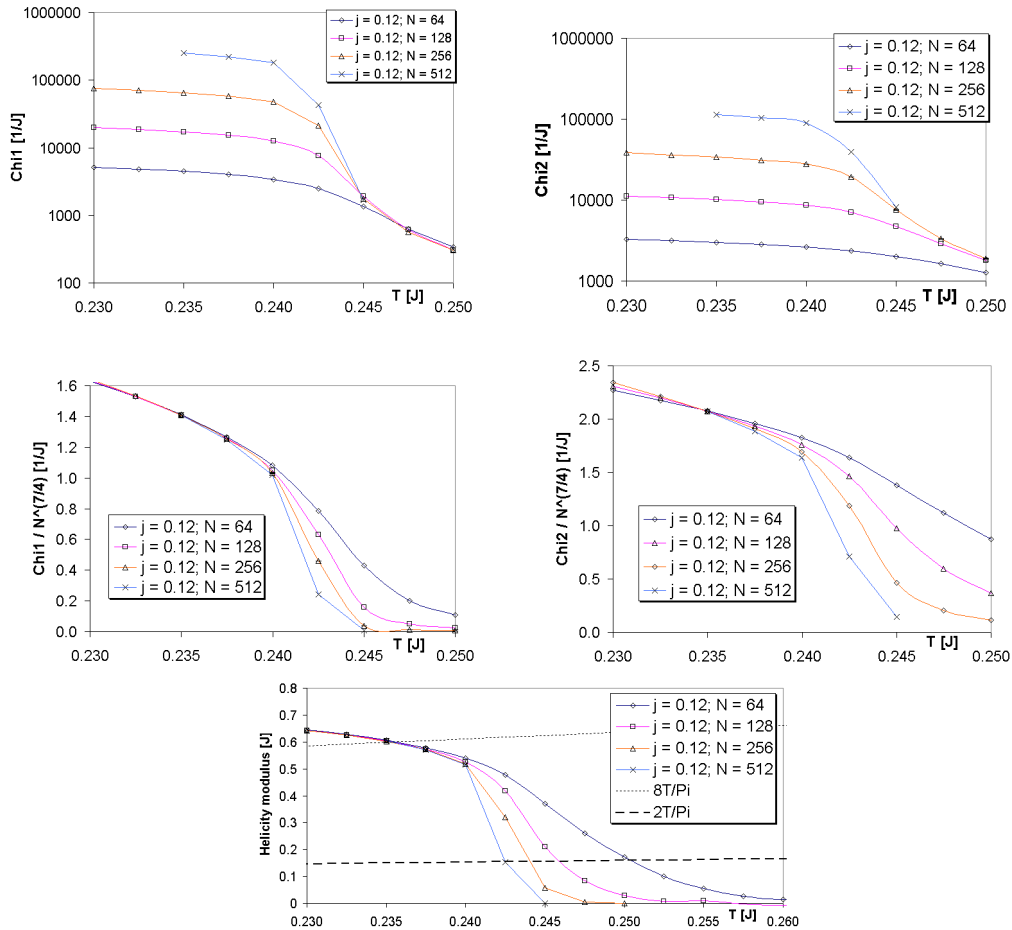


Figure 4.15: Above: The magnetic susceptibility $\chi_{1,N}(T)$ and the nematic susceptibility $\chi_{2,N}(T)$ for $N = 64, 128, 256, 512$ and $j = 0.12$. In the middle: The finite-size scaling of the magnetic susceptibility $\chi_1 N^{7/4}$ intersects quite well at $T_2(j = 0.12) \approx 0.2325 J$. The finite-size scaling of the nematic susceptibility $\chi_2 N^{7/4}$ intersects quite well, too. Below: The jump of the helicity modulus $\Upsilon_N(T)$ for $j = 0.12$ does not look as $\frac{2T}{\pi}$, nor as $\frac{8T}{\pi}$.

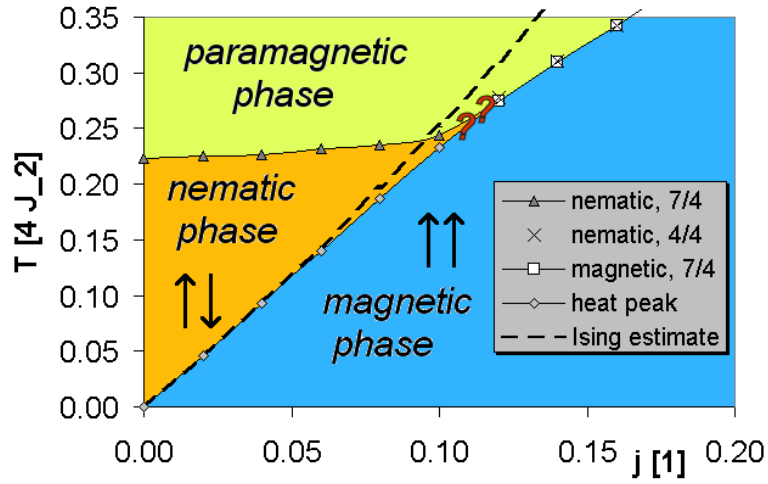


Figure 4.16: Phase diagram in the most interesting region of the j, T plane. The magnetic-nematic phase transition temperature $T_1(j)$ was obtained from the specific heat peaks for various j . The Ising estimate of phase transition temperature $T_1(j)$ (see Eq.(1.20)) is plotted there for comparison. The nematic-paramagnetic phase transition temperature $T_2(j)$ was found using the finite-size-scaling for the nematic susceptibility as the intersection of $\chi_{2,N}(T) N^{7/4}$ for various lattice sizes N . The magnetic-paramagnetic phase transition was determined using the finite-size scaling of both susceptibilities as the intersection of $\chi_{1,N}(T) N^{7/4}$, or $\chi_{2,N}(T) N^{4/4}$ for various N . The region near the triple point was not inspected seriously.

Conclusion

We have studied a modified 2-dimensional XY model on the square lattice defined by the Hamiltonian

$$H = - \sum_{\langle kl \rangle} [J_1 \cos(\theta_k - \theta_l) + J_2 \cos 2(\theta_k - \theta_l)], \quad \text{for } J_2 \geq 0,$$

using Monte Carlo simulations. Our goal was to specify the phases in the space of coupling parameter $j = \frac{J_1}{J_1 + 4J_2}$ and temperature T and to determine the types of phase transitions between the phases. We have revised the KT theory for our modified model.

We have verified the expectation that the phase diagram consists of 3 phases (the magnetic, the nematic and the paramagnetic phase) by measuring the helicity modulus and the magnetic and the nematic susceptibility. The character of the phase transitions was investigated in detail for 4 representative values of the parameter j , namely $j = 0, 0.02, 0.16, 1$.

The phase transition between the magnetic and the nematic phase is Ising-like. We have 2 arguments (1-2) and 3 indications (3-5) in support of this:

1. The peak of the differential heat capacity scales, within the error bars, as it should for the Ising model.
2. We have found an order parameter m , which scales in close vicinity of T_1 as $(T_1 - T)^\delta$ with the Ising exponent $\delta = 1/8$.
3. The entropy increase according to the differential heat capacity is with high accuracy $\ln 2$.
4. The Ising-estimate Eq.(1.20) of $T_1(j)$ fits well the determined transition temperatures $T_1(j)$.
5. The number of walls increases at the transition temperature T_1 rapidly.

The transition between the magnetic and the paramagnetic phase is of the Kosterlitz-Thouless (KT) type with an universal jump $\frac{2T}{\pi}$ caused by unbinding of vortex-anti-vortex pairs. We have investigated the phase transition using finite-size scaling of the helicity modulus Υ , the magnetic susceptibility χ_1 , and of the nematic susceptibility χ_2 , the transition temperatures were internally consistent. From the finite-size scaling of the helicity modulus it is observable that the magnitude of the universal jump is $\frac{2T}{\pi}$ with reasonable accuracy.

The nematic-paramagnetic transition is of the KT type with an universal jump $\frac{8T}{\pi}$ caused by unbinding of half-vortex-anti-half-vortex pairs. We have studied the finite-size scaling of the helicity modulus and of the nematic susceptibility and the obtained transition temperatures were internally consistent. Again, the helicity modulus reveals that the value of the universal jump is close to $\frac{8T}{\pi}$.

Slovak summary

Slovenský súhrn

V tejto práci sme študovali modifikovaný XY model na štvorcovej mriežke definovaný Hamiltoniánom

$$H = - \sum_{\langle kl \rangle} [J_1 \cos(\theta_k - \theta_l) + J_2 \cos 2(\theta_k - \theta_l)], \quad \text{pre } J_2 \geq 0.$$

Naším cieľom bolo pomocou Monte Carlo simulácií určiť fázový diagram v rovine parametra $j = \frac{J_1}{J_1 + 4J_2}$ a teploty T a charakter fázových prechodov medzi jednotlivými fázami.

Prevažná väčšina dát bola získaná pomocou randomizovaného Wolff-ovho algoritmu, menšia časť pomocou Metropolis-ovho algoritmu. Naš modelový systém tvorili štvorcové mriežky $N \times N$ spinov s periodickými okrajovými podmienkami, typicky pre $N = 64, 128, 256, 512$. Simulácie odhalili pomocou meraní tuhosti spinov Υ a magnetickej, resp. nematickej susceptibility χ_1, χ_2 , že fázový diagram pozostáva z 3 fáz: magnetickej, nematickej a paramagnetickej.

Prepracovali sme teóriu Kosterlitz-a a Thouless-a [2] pre náš model a teoreticky sme podchytili charakter KT fázových prechodov pre prechod magnet-paramagnet a nematikum-paramagnet. Kvalitatívne sme ukázali, že prechod medzi magneticou a nematickou fázou môže byť Ising-ovského typu.

Jednotlivé typy fázových prechodov sme preverovali pre tzv. reprezentatívne rezy parametrickej roviny, konkrétne pre $j = 0, 0.02, 0.16, 1$. Hodnoty parametra j boli zvolené tak, aby pokrývali všetky fázové prechody.

Našli sme 2 argumenty (1-2) a 3 indície (3-5) dokladajúce, že prechod medzi magnetom a nematikom je Isingovský:

1. Maximum mernej tepelnej kapacity (na 1 spin) $c_{\text{diff}}(T)$ prislúchajúci interakcii J_2 (t.j. energii doménových stien) rastie s veľkosťou mriežky v rámci neistôt meraní logaritmicky s veľkosťou, tak ako je to známe pre Ising-ov model.
2. Našli sme parameter usporiadania m , ktorý škáluje v tesnej blízkosti pod T_1 proporcionálne s $(T_C - T)^\delta$, kde $\delta = 1/8$ je exponent pre Ising-ov prechod.
3. Nárast entropie prislúchajúci mernej tepelnej kapacite $c_{\text{diff}}(T)$ je s vysokou presnosťou $\ln 2$.
4. Odhad Eq.(1.20) pre teplotu $T_1(j)$ Ising-ovského prechodu je vo výbornom súlade s výsledkami simulácií.
5. Počet doménových stien pri teplote prechodu T_1 prudko stúpa.

Fázový prechod medzi magneticou fázou a paramagneticou fázou je podľa nás spôsobený prítomnosťou viazaných párov vĺr-antivĺr, ktoré sa pri kritickej teplote prechodu stávajú voľnými vĺrmi. Pre tento fázový prechod KT teória predpovedá univerzálny skok v tuhosti spinov o $\frac{2T}{\pi}$. Tento skok je zo škálovania tuhosti spinov pre rôzne mriežky dobre badateľný. Teploty fázového prechodu sme určovali zo škálovania tuhosti spinov, magnetickej a nematickej susceptibility. Takto určené teploty fázového prechodu boli konzistentné, čo je netriviálny výsledok prispievajúci k potvrdeniu predpokladu, že tento prechod je typu KT, a že je spôsobený rozpadom párov vĺr-antivĺr.

Za fázový prechod medzi nematikom a paramagnetom sú podľa našej teórie zodpovedné polvĺry, ktoré sa v nematickej fáze vyskytujú iba viazané v pároch a v paramagnetickej sú už voľné. Skok v tuhosti je pre takýto KT prechod tiež univerzálny, $\frac{8T}{\pi}$. Na reprezentatívnych vzorkách $j = 0, 0.02$ sme urobili škálovanie tuhosti spinov a nematickej susceptibility a dostali sme konzistentné teploty fázového prechodu, čo je opäť pozitívny test teórie.

Bibliography

- [1] R. E. Peierls, *Helv. Phys. Acta* **7**, 81 (1934).
- [2] J. M. Kosterlitz and D. J. Thouless, *J. Phys. C: Solid State Phys.* **6**, 1181 (1973).
- [3] R. Hlubina, *Phys. Rev. B* **77**, 094503 (2008).
- [4] K. Zhao, C. Harrison, D. Huse, W. B. Russel, and P. M. Chaikin, *Phys. Rev. E* **76**, 040401 (2007).
- [5] A. P. Young, *J. Phys. C: Solid State Phys.* **11**, L453 (1978).
- [6] P. Minnhagen and B. J. Kim, *Phys. Rev. B* **67**, (2003).
- [7] P. Minnhagen and G. G. Warren, *Phys. Rev. B* **24**, 2526 (1981).
- [8] N. Metropolis, A. W. Rosenbluth, M. N. Rosenbluth, A. H. Teller, and E. Teller, *J. Chem. Phys.* **21**, 1087 (1953).
- [9] U. Wolff, *Phys. Rev. Lett.* **62**, 361 (1989).
- [10] Wikipedia, 2009, [http://en.wikipedia.org/wiki/Standard_error_\(statistics\)](http://en.wikipedia.org/wiki/Standard_error_(statistics)).
- [11] J. Tobochnik and G. V. Chester, *Phys. Rev. B* **20**, 3761 (1979).
- [12] H. Weber and P. Minnhagen, *Phys. Rev. B* **37**, 5986 (1988).
- [13] P. Olsson, *Phys. Rev. B* **52**, 4526 (1995).
- [14] M. Hasenbusch, *J. Phys. A: Math. Gen.* **38**, 5869 (2005).
- [15] J. P. Sethna, *Entropy, Order Parameters, and Complexity* (Clarendon Press, Oxford, 2009), p. 270.
- [16] A. E. Ferdinand and M. E. Fisher, *Phys. Rev.* **185**, 832 (1969).